Structural Fluctuations of the *Escherichia coli* Co-chaperonin GroES Studied by the Hydrogen/Deuterium-Exchange Methods

Mahesh Shantilalji Chandak

Department of Functional Molecular Science,

School of Physical Sciences,

The Graduate University for Advanced Studies (Sokendai)

A dissertation submitted for the degree of Doctor of Philosophy

Abstract

The thesis consists of four chapters, **Chapter 1.** "General introduction," **Chapter 2.** "The use of spin desalting columns in DMSO-quenched H/D-exchange NMR experiments," **Chapter 3.** "The H/D-exchange kinetics of the *Escherichia coli* (*E. coli*) co-chaperonin GroES studied by 2D NMR and DMSO-quenched exchange methods," and **Chapter 4.** "Summary and future perspectives."

In Chapter 1, I describe general introduction about protein folding, molecular chaperones and hydrogen-exchange techniques. For proper biological functions of proteins, they have to fold into the native three-dimensional (3D) structures. How a protein folds from its primary structure into the native 3D structure has been a major research interest in the field of biophysical, biochemical and biomedical sciences. As the interior of biological cell is very much crowded, the cytoplasm does not serve as an ideal place for protein folding, and there exist machineries which assist protein to fold into the native state *in vivo*, and such machineries are called "molecular chaperones." Among all chaperones, the GroEL/GroES complex, found in *E. coli*, is one of the extensively studied molecular chaperones. The GroEL/GroES chaperonin complex is very huge with the co-chaperonin GroES of a molecular weight of 73 kDa (7 subunits) and GroEL of a molecular weight of 800 kDa (14 subunits), resulting in the megadalton chaperonin machinery. There are a number of studies on the GroEL/GroES complex, but the structural flexibility and fluctuations of the chaperonin complex remains to be understood. For free heptameric GroES and the GroES portion of the GroEL/GroES complex, however, it is quite feasible to characterize the structural fluctuations by the hydrogen/deuterium (H/D)-exchange methods combined with two-dimensional (2D) nuclear magnetic resonance (NMR) spectroscopy, although we still need sophisticated new techniques to overcome low quality of the GroES spectra taken by the conventional NMR techniques. The use of the H/D-exchange methods can shed light on the

structural flexibilities and dynamic behavior of the GroEL/GroES complex. In the H/D-exchange methods, the peptide amide protons are exchanged with solvent deuterons at every amino-acid residue, and the H/D-exchange reactions can be monitored as time-dependent changes in the amide-proton signals by NMR spectroscopy. With the help of observed H/D-exchange rate constants and predicted theoretical H/D-exchange rate constants, we can easily evaluate protection factors for the individual amino-acid residues, which ultimately gives us crucial information about the structural fluctuations and dynamics of the chaperonin complex. Hence, the general introduction of Chapter 1 gives brief descriptions of these aspects.

In Chapter 2, I describe a new method, which I developed for measurement of H/D-exchange kinetics, i.e., the use of spin desalting columns in dimethylsulfoxide (DMSO)-quenched H/D-exchange NMR experiments. The DMSO-quenched H/D-exchange (DMSO-QHX) method is a powerful method to characterize the H/D-exchange behaviors of proteins and protein assemblies, and it is potentially useful for investigating non-protected fast-exchanging amide protons in the unfolded state. However, this method has not been used for studies on fully unfolded proteins in a concentrated denaturant or protein solutions at high salt concentrations. In all of the current DMSO-QHX studies of proteins so far reported, lyophilization was used to remove D_2O from the protein solution, and the lyophilized protein was dissolved in the DMSO solution to quench the H/D-exchange reactions and to measure the amide proton signals by 2D NMR spectra. The denaturants or salts remaining after lyophilization thus prevent the measurement of good NMR spectra. In this new method, I found that the use of spin desalting columns is a very effective alternative to lyophilization for the medium exchange from the D_2O buffer to the DMSO solution. In this method, the medium exchange by a spin desalting column took only about 10 min in contrast to an overnight length of time required for lyophilization, and the use of spin desalting columns has made it possible to monitor the H/D-exchange behavior of a fully

unfolded protein in a concentrated denaturant. I analyzed H/D-exchange kinetics of the unfolded ubiquitin in 6.0 M guanidinium chloride and related results are discussed in Chapter 2.

In Chapter 3, I studied H/D-exchange reactions of peptide amide protons of free heptameric GroES complex. To map H/D-exchange kinetics, I used two different techniques: (1) 2D ^{1}H–^{15}N transverse-optimized NMR spectroscopy and (2) the DMSO-QHX method combined with conventional ^{1}H–^{15}N heteronuclear single quantum coherence (HSQC) spectroscopy. By using these techniques together with direct HSQC experiments, I quantitatively evaluated the exchange rates for 33 out of the 94 peptide amide protons of GroES and their protection factors, and for the remaining 61 residues, I obtained the lower limits of the exchange rates. The protection factors of the most highly protected amide protons were on the order of 10^{6}–10^{7}, and the values were comparable in magnitude to those observed in typical small globular proteins, but the number of the highly protected amide protons with a protection factor larger than 10^{6} were only 10, significantly smaller than the numbers reported for small globular proteins, indicating that the significant portions of free heptameric GroES are flexible and natively unfolded. The highly protected amino-acid residues with a protection factor larger than 10^{5} were mainly located in three β-strands that form the hydrophobic core of GroES, while the residues in a mobile loop (residues 17–34) were not highly protected. The protection factors of the most highly protected amide protons were orders of magnitude larger than the value expected from the equilibrium unfolding parameters previously reported, strongly suggesting that the equilibrium unfolding of GroES is more complicated than a simple two-state or three-state mechanism and may involve more than a single intermediate.

In Chapter 4, I summarize the present study and discuss future perspectives. Development of the spin-column technique was very useful to follow the H/D-exchange kinetics of free GroES and the GroEL/GroES complex, whose solutions contained certain amounts of salts, as well as to study fully unfolded ubiquitin in 6.0 M guanidinium chloride. The H/D-exchange protections

were mostly observed in strands B, C and D of free heptameric GroES, but the mobile loop region formed by residues 17–34 and the reverse turn formed by residues 49–52 were not highly protected against the H/D-exchange. Hence, these results of Chapters 2 and 3 are summarized in this chapter. In addition, I also describe preliminary results of the H/D-exchange kinetics of the GroES complexed with a single ring mutant (SR1) of GroEL in the presence of ADP. In this preliminary study of the SR1/GroES complex, I observed significant protections (protection factors of 10^5–10^6) for the amide protons in the mobile loop region (residues 17–34), indicating that the mobile loop is highly organized and plays a significant role when the co-chaperonin GroES forms a complex with SR1. Thus, the study in my thesis has overall clarified detailed changes in the dynamic behaviors of the GroES portion of the GroEL/GroES chaperonin complex.

Abbreviations:

DMSO : Dimethylsulfoxide

H/D : Hydrogen/deuterium

NMR : Nuclear magnetic resonance

1D : One-dimensional

2D : Two-dimensional

3D : Three-dimensional

HSQC : Hetero-nuclear single quantum coherence

GdmCl : Guanidinium chloride

DCA : Dichloroacetic acid

E. coli : *Escherichia coli*

TROSY : Transverse relaxation-optimized spectroscopy

RF : Radio-frequency

FID : Free induction decay

T_2 : Transverse-relaxation time

DD : Dipole-dipole interactions

CSA : Chemical shift anisotrophy

Cyt *c* : Cytochrome *c*

PDB : Protein data bank

HPLC : High-performance liquid chromatography

N_7 : Native heptameric GroES

U : Unfolded monomeric GroES

M : Folded monomeric GroES.

Tris : Tris (hydroxymethyl) aminomethane

DMSO-QHX : DMSO-quenched H/D-exchange

P_f : Protection factor

k_{open} : The rate constant for structural opening

k_{close} : The rate constant for structural closing

SR1 : A single ring mutant of GroEL

ΔG_{eff} : The effective Gibbs free-energy change of unfolding

k_{int} : The intrinsic exchange rate constant

K_U : The equilibrium constant of unfolding

K_d : The equilibrium dissociation constant

ΔG_U : The Gibbs free-energy change of unfolding of GroES per monomer unit

EDTA : Ethylenediaminetetraacetic acid

Thesis contents

Chapter 1. General introduction

1.1. Protein folding

For proper functions of proteins, they have to fold into the correct native 3D structures. From decades ago, the protein folding problem has been evolved as a key area of research interest in molecular biology, biochemistry and biophysics. How a protein folds from the primary structure into its functionally active native 3D conformation is still a most important question in biological sciences.

In early 1960s, Anfinsen and his co-workers[1] worked on ribonuclease A, and they have shown that the native structure of the protein is thermodynamically most stable (thermodynamic hypothesis) and that it is attained only by the primary structure (genetic information), i.e., no additional information is required for attaining the native structure. The thermodynamic hypothesis thus states that the 3D structure of a native protein in its normal physiological milieu (solvent, pH, ionic strength, presence of other components such as metal ions or prosthetic groups, temperature, and other) is the one in which the Gibbs free energy of the whole system is lowest, that is, the native conformations are determined by the totality of interactions and hence by the amino-acid sequence, in a given environment.

However, the thermodynamic hypothesis alone is not enough to elucidate the molecular mechanisms of protein folding. For example, a protein of 100 residues will have 99 peptide bonds, which means that it will have 198 backbone dihedral angles (99 ϕ and 99 ψ angles). If every dihedral angle takes one out of three possible conformations, then there are 3^{198} (= 3.0×10^{94}) possible conformations for the whole molecule. So, if the protein has to experience all these possible conformations by random search before it reaches to the unique native state (this does not violate the thermodynamic hypothesis), the time required for folding will be much longer than the time of the universe, i.e., the protein can never fold. In 1968, Cyrus Levinthal[2] proposed this paradox (Levinthal's paradox), which states that although a protein generally has a

vast size of the conformational space, the protein can search and attain the native state very quickly; sometimes the time required for folding is as short as microseconds. Therefore, the protein takes only a very limited number of its possible conformations during folding. Levinthal thus proposed that there is a specific pathway of folding and that this specific pathway is also encoded in the amino-acid sequence.

If there is the specific pathway of folding, there must be specific folding intermediates along the folding pathway. Major objectives of experimental studies of protein folding are to detect and characterize such folding intermediates. However, the folding intermediates lives for a very short period of time often less than 1 s, so that it is very difficult to isolate and study them by conventional biophysical techniques. To detect and characterize the transient folding intermediates, we thus use a variety of kinetic techniques, including stopped-flow circular dichroism, stopped-flow fluorescence, stopped-flow X-ray scattering, and H/D-exchange labeling 2D NMR techniques. Until now, several different models of protein folding have been proposed on the basis of the experimental results so far reported, and these models may include a framework model, a hydrophobic-collapse model, and a nucleation-condensation model.[3]

Another view that also resolves the Levinthal's paradox is a funnel theory, which was first proposed by Onuchic and Wolynes in early 1990s.[4] In the funnel theory, the protein folding is represented as a trajectory in a conformation-energy hyperspace that represents the energy landscape of protein conformations. In the funnel theory, a protein can fold into the native conformation, because there is always an energy bias toward the native conformation everywhere in the conformation-energy hyperspace. The funnel theory is quite popular in the theoretical and computational studies of protein folding, but it is difficult to determine a real shape of the folding funnel by experiments.

1.2. Chaperonin — folding machinery

The interior of biological cell is very much crowded, and the effective concentration of a proteins in *E. coli* cells has been estimated as high as ~300 mg/ml.[5] Because of such high concentrations of proteins and several other biomolecules, the cytoplasm does not serve as an ideal place for protein folding. Protein folding at such a high concentration results in irreversible aggregation between protein molecules that have not yet fully folded. Therefore, there exist proteinous molecular machineries that assist other proteins to fold into the native state by preventing the irreversible aggregations. Such machineries are called as "molecular chaperones", and the molecular chaperones are also required for degradation, translocations and repair of various proteins *in vivo*.[6, 7] Among various molecular chaperones, the chaperonin is quite unique and specialized for assisting protein folding. It has a ring-like structure, consisting of the tetradecameric or hexadecameric protein supermolecular complex with a central cavity. A primary role of the chaperonin is thus to bind non-native proteins and trap them inside the cavity to assist the folding by segregating immature folding intermediates from crowded external environment. Protein folding, maintenance of proteome integrity, and protein homeostasis (proteostasis) critically depend on a complex network of molecular chaperones.[8]

There are two types of the chaperonin, the group I and the group II chaperonins. They have similar double-ring structures with each ring consisting of seven subunits for the group I and eight or nine subunits for the group II chaperonin, but they are different in the amino-acid sequence. The group I chaperonins (chaperonin 60s) are found in eubacteria such as *E. coli* and in the mitochondria and the chloroplast of eukaryotic cells, and the best-characterized group I chaperonin is GroEL of *E. coli.* The group I chaperonin has its partner protein (chaperonin 10), which act as a lid when it binds to chaperonin 60. Chaperonin 10 is also called co-chaperonin, and the co-chaperonin of GroEL is GroES. The group II chaperonins are found in the cytosol of

the Eukarya and the Archaea, and they are hetero-oligomeric. The group II chaperonin does not have the co-chaperonin, but it has a helical protrusion in the apical domain of the chaperonin subunit itself, and the helical protrusions of the chaperonin ring function like a lid to encapsulate a substrate protein.[9,10] The eukaroytic chaperonin, TRiC or CCT, contains eight different subunits per ring with each subunit having molecular weight of 50 to 60 kDa, whereas the archeal thermosome consists of one to three different subunits, which are arranged in eight- or nine-member symmetrical rings.[9,11] They also assists protein folding *in vivo* in an ATP-dependent manner, and the folding-assisting mechanism of the group II chaperonins are less understood than that of the group I chaperonins.

1.2.1. GroEL/GroES complex

Figure 1-1 shows the overall architecture of GroEL/GroES complex. The *E. coli* chaperonin complex, GroEL/GroES, is a widely studied chaperonin, consisting of 14 subunits of GroEL (M_w = 58 kDa for a subunit) and 7 subunits of GroES (M_w = 10.4 kDa), adding up to the total molecular weight of 882 kDa.[12] The chaperonin GroEL/GroES assists at least 250 different cytosolic proteins to fold into the native state in *E. coli*.[13] In the presence of ADP or ATP, the GroEL/GroES complex is formed, and the GroES ring acts as a lid in the complex. ATP binds tightly and is hydrolyzed on only one heptameric ring of the GroEL at a time, thus inducing allosteric transition in the GroEL oligomer even in the absence of GroES.[14] In addition, allosteric transitions are induced by metal fluoride-ADP complex, an analogue of ATP.[15] A non-native protein is encapsulated within the central cavity of the GroEL/GroES complex, and then it is released. This process takes a half time of about 10 to 30 s.[16]

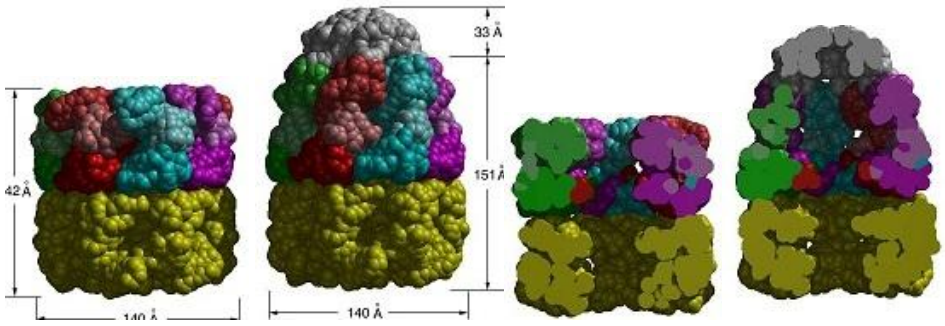

Figure 1-1. Overall architecture and dimensions of GroEL and GroEL-GroES-$(ADP)_7$. Van der Waals space-filling models (6 Å spheres around C^{α}) of GroEL (*left*) and GroEL-GroES-$(ADP)_7$ (*right*). The left panel shows the outside view, showing outer dimensions, and the right panel shows the insides of the assembly and was generated by slicing off the front half with a vertical plane that contains the cylindrical axis. Various colors are used to distinguish the subunits of GroEL in the upper ring. The domains are indicated by *shading*: equatorial, *dark hue*; apical, *medium hue*; intermediate, *light hue*. The lower GroEL ring is *uniformly yellow*. The figure was taken from Sigler *et al*. with permission.[17]

GroES

GroES is a heptameric (seven-member ring) complex, having each subunit with a molecular weight of 10.4 kDa. The GroES crystal structure was determined at 2.8 Å, and it has a dome-like structure, approximately 75 Å in diameter and 30 Å in height, with an 8 Å orifice in the center of its roof.[19] GroES contains two loop regions, a flexible mobile loop of residues 17–34, which is involved in the binding to GroEL,[19-21] and a roof hairpin loop of residues 44–58.[19] Electron-micrographic studies have shown that GroES is placed at the top of one polypeptide binding chamber of GroEL to form a stable $GroES_7$-$GroEL_{14}$-ADP_7 complex.[12, 22] Figure 1-2 shows schematic representation of the monomeric subunit of GroES.

The binding of GroES triggers conformational changes both in the GroES adjacent end and at the opposite end of the GroEL cylinder, which prohibits the association of a second GroES oligomer. A substrate polypeptide and GroES bind to the same ring of GroEL and released after ATP hydrolysis.[23, 24]

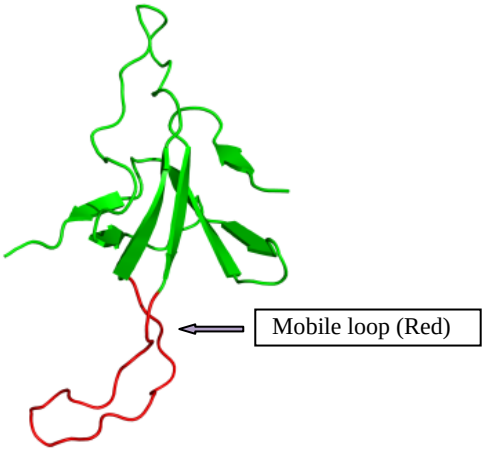

Figure 1-2. Ribbons drawing of one subunit in the GroES ring .

GroEL

GroEL is a thick-walled cylinder of 140 Å in a height and of 135 Å in an outer diameter, and it is thus hollow with the central cavity.[18] The monomer subunit of GroEL consists of 547 amino acids arranged in three different domains: (1) The apical domain, which is locally more flexible than the other domains, has binding sites for substrate proteins and GroES, and is considerably less well ordered; (2) the intermediate domain, which connects the apical and equatorial domains; and (3) a well-ordered, highly α-helical, "equatorial" domain, which provides residues for the inter- and intra-ring interactions of the protein complex, and it also contributes most of the residues that constitute the binding site for ADP and ATP. [17]

Formation of the GroEL/GroES Complex

As shown in Figure 1-3, in the presence of ADP or ATP, the GroEL/GroES complex is formed. There are two kinds of the GroEL/GroES complex, one is the asymmetric $GroEL_{14}$-$GroES_7$ complex called a "bullet-type" complex, whereas the other is the symmetric $GroES_7$-$GroEL_{14}$-$GroES_7$ complex called a "football-type" complex. The football-type complex is formed when both rings of GroEL are occupied by ATP. Schematic model for football and bullet type GroEL/GroES complex is shown in Figure 1-4.

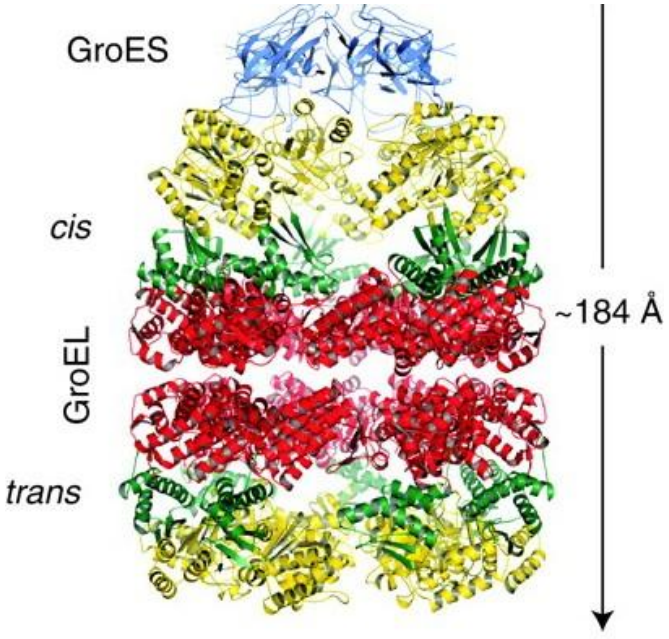

Figure 1-3. The crystal structure of the asymmetric GroEL/GroES complex (PDB code: 1AON). *Cis*, the GroES-bound chamber of GroEL, and *trans*, the opposite GroEL ring. The figure was taken from Hartl *et al.* with permission.[27]

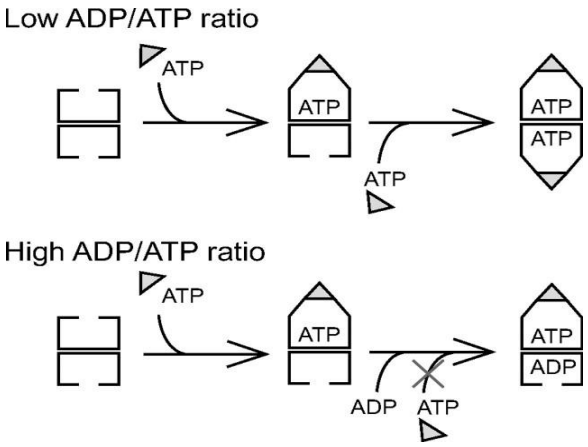

Figure 1-4. A schematic model for the reaction mechanism of GroEL and GroES. The figure was taken from Sameshima *et al.* with permission.[39]

However, the hydrolysis of ATP to ADP inhibits the binding of another ATP with the trans-ring of the bullet-type complex, and as a result, the second GroES does not bind to the trans-ring of GroEL.[25] Protein folding in chaperonin is based on successive rounds of binding and release, and partitioning between committed and kinetically trapped intermediates.[26]

1.2.2. The GroEL/GroES reaction cycle

Figure 1-5 indicates overall GroEL/GroES reaction cycle, the reaction cycle of GroEL/GroES association is highly dynamic. The binding of ATP to GroEL is the primary requirement for binding of GroES to GroEL, and the binding and hydrolysis of ATP leads to the series of conformational changes in the apical domain of GroEL. At a physiological concentration of ATP (~1 mM), GroEL binds to ATP cooperatively within the seven sites of one ring. Upon binding of ATP, the apical domains tilt together with the intermediate domains, begin to elevate themselves, then detach from each other, expand radially, and finally elevate further

for the binding of a substrate protein.[28] The substrate protein binds to the tilting and elevating domains of GroEL, and the simultaneous binding of the nonnative substrate protein by the C-terminal tails and the lower segments of the cis apical domains provides a mechanism for retaining the bound nonnative substrate protein while the GroEL ring shifts into another state to permit loading of GroES.[22] As the binding of GroES is dependent on ATP, the GroES will rapidly bind to the same ring of GroEL, where ATP is bound, whereas the other end of GroEL remains accessible to the substrate polypeptide.[23, 29] The GroES binding to GroEL leads to a doubling in volume of the central cavity in the bound GroEL ring, and as a result, major conformational changes in the apical domains of GroEL occur. The apical domains then rotate upward to make contact with the mobile loops of the GroES ring. After docking of GroES, the apical domains of GroEL elevate, and the massive twist provides a power stroke of the chaperonin movement, which ejects the substrate protein to collapse inside the final folding chamber.[28]

The surface residues of GroEL are highly mobile, so that it can accommodate various non-native folding intermediates or unfolded proteins and a wide variety of substrates that expose hydrophobic surfaces.[30, 31] The interaction between GroEL and the substrate has been proposed to be largely hydrophobic because GroEL interacts with proteins in non-native conformations but not in native forms.[32] It has been found that mutations from hydrophobic to hydrophilic residues in the surface region lead to unfunctional GroEL, i.e., it doesn't assist protein folding.[33]

The interior surface of the trans ring of GroEL consists of hydrophobic amino acids, but the conformational transitions of GroEL induced by the GroES binding change the inner surface of the central cavity from hydrophobic to hydrophilic residues. Therefore, the non-native protein inside the cavity of the GroEL/GroES complex then gets surrounded by the hydrophilic environment, and this opens up a chance for the substrate protein to fold into the native state.[12]

The folding of the substrate protein takes place in the cis cavity of the GroEL/GroES/ATP complex, and there is ATP hydrolysis in the cis ring, weakening the affinity of GroEL for GroES. Then, the binding of ATP at the trans ring of the GroEL/GroES/ADP complex takes place, further weakening the interaction between GroEL and GroES, and this gives a signal for substrate-polypeptide (ligand) release and the release of GroES and ADP.[26, 34]

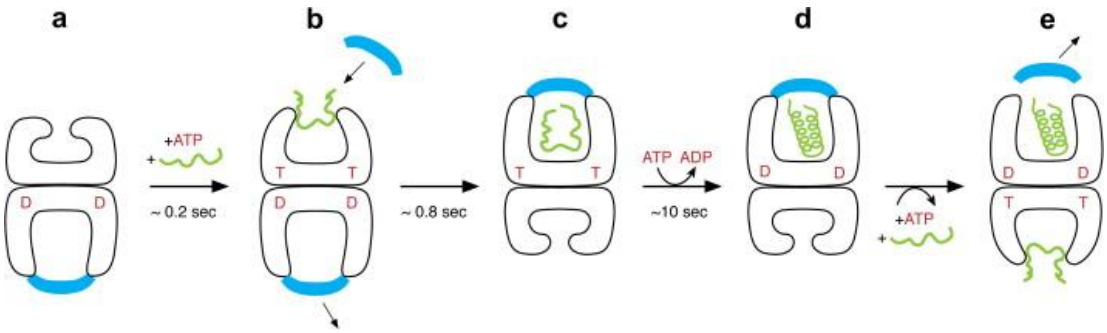

Figure 1-5. The chaperonin reaction cycle- An asymmetric GroEL/GroES/ADP complex (a) is the normal acceptor state for ATP (red; also indicated as T) and a non-native polypeptide (green), and they bind to the open ring opposite the one bound by GroES (blue) and ADP (red D) (b). ATP binding produces small rigid-body domain movements of the apical domains in the bound ring (b), enabling GroES binding, attended by large rigid body movements that produce the stable folding-active cis complex end-state (c). This folding-active state is the longest-lived state of the reaction cycle, ~10 s, followed by ATP hydrolysis (c → d), which then gates the entry of ATP and polypeptide into the opposite trans ring, rapidly discharging the cis ligands (e) and initiating a new folding-active cycle on the ATP/polypeptide-bound ring. The figure was taken from Horwich *et al*. with permission.[37]

An inward tilt of the cis equatorial domain causes an outward tilt in the trans ring, and the ATP binding is thus cooperative within one ring and anti-cooperative between the two rings,

which allows alternative folding in the two chambers, i.e., the substrate enclosure in one ring leads to the substrate release in the other ring Thus, the two rings of GroEL acts in an anti-cooperative manner, favoring binding of ATP and GroES at only one ring at one time.[12, 35, 36] Upon ATP binding to the trans ring of the complex, GroES leaves first, followed by the ligand release in any of the three conformational states: the native state, a conformational state that is highly committed to reach at the native state, and a non-native state. All non-native polypeptides again bind to GroEL for the next trial to fold into the native state.[23, 26, 37]

The binding of ATP at the trans ring also triggers binding of non-native substrate protein and GroES, thus converting it into the new cis ring, and this chaperonin cycle continues until the non-native protein is fully folded into the native state.[38]

1.3. Hydrogen-exchange techniques

Structural fluctuations and dynamics of proteins are important factors to control proper biological functions of proteins, and alterations in these properties may result in malfunctions of proteins. The H/D-exchange technique is a unique experimental technique by which we can detect protein's small structural fluctuations, which cannot be observed by conventional spectroscopic and other biophysical techniques.

In addition, this technique is also useful to study chemically or physically denatured states, and equilibrium or kinetic folding intermediates, in which direct determination of 3D structure is not possible. In the hydrogen-exchange method, we measure exchange reactions of peptide amide protons of a protein with protons of solvent water. When we use heavy water (deuterium oxide, D_2O) as a solvent, the H/D-exchange reaction can be monitored by ^{1}H NMR spectroscopy as time-dependent changes in the amide-proton signals. Uniformly ^{15}N-labeled proteins and ^{1}H–

^{15}N HSQC- NMR spectra are often used for this purpose. The H/D-exchange reaction of the peptide amide proton thus takes place at every amino acid position except proline residues which do not have the amide group. Along with the peptide amide groups, the protons in polar side chains are also exchanged with solvent deuterons, but they are often exchanged too rapidly to monitor by the HSQC spectra.

1.3.1. The mechanisms of the H/D exchange

The H/D-exchange reaction of a freely exposed amide proton in D_2O is expressed by

$$\text{N-H} + \text{D}_2\text{O} \xrightarrow{k_{int}} \text{N-D} + \text{DOH} \qquad (1\text{-}1)$$

where k_{int} is the intrinsic rate constant for the chemical H/D-exchange process of the amide group. The exchange reaction of a particular amide group can be sterically blocked by neighboring bulky side chains or induced by neighboring polar side chains; therefore, the exchange rates of individual amides vary with the amino acid sequence.[40] The k_{int} value is affected by various factors, including pH, temperature, and inductive and steric effects of side chains.[41, 42] If all these factors are taken into consideration, we can calculate the intrinsic exchange rates of individual amide protons of a protein from its amino-acid sequence. The methods of Bai *et al.*[43] and Connelly *et al.*[44] are usually used for calculating the k_{int} values from the amino-acid sequence of a protein. The actual observed exchange rate, k_{ex}, of a folded native protein is also affected by the 3D protein structure and structural fluctuations, and at neutral pH and room temperature, the half time of the H/D-exchange ranges from milliseconds to months.

The H/D-exchange kinetics of a native protein is interpreted by a three–state model, in which we assume the presence of three states, (1) a non-exchangeable state (NH_{closed}), in which the amide proton is protected from the H/D-exchange, (2) an exchangeable state (NH_{open}), in which

the amide proton is freely exposed to solvent and exchanged with solvent deuteron with an intrinsic exchange rate constant k_{int}, and (3) an exchanged state ($ND_{exchanged}$), in which the amide proton is already exchanged with solvent deuteron, this model is represented as

$$NH_{closed} \underset{k_{close}}{\overset{k_{open}}{\rightleftharpoons}} NH_{open} \xrightarrow{k_{int}} ND_{exchanged} \qquad (1\text{-}2)$$

where, k_{open} is the rate constant for structural opening, which makes the amide proton fully accessible to solvent, and k_{close} is the rate constant for structural closing, which fully protects the amide proton from the H/D-exchange. Therefore, in this model, there are opening-closing equilibria for individual amide protons in a protein, and the equilibrium constant for the opening reaction (K_{open}) is given by

$$K_{open} = k_{open} / k_{close} \qquad (1\text{-}3)$$

The opening reaction of a native protein is brought about by local structural fluctuations, by partial unfolding, and sometimes also by global unfolding of the protein. By assuming the steady state in Equation (1-2), the observed exchange rate constant k_{ex} is represented by

$$k_{ex} = k_{open} \cdot k_{int} / (k_{open} + k_{close} + k_{int}) \qquad (1\text{-}4)$$

Because $k_{close} \gg k_{open}$, it follows that

$$k_{ex} = k_{open} \cdot k_{int} / (k_{close} + k_{int}) \qquad (1\text{-}5)$$

There are two limiting mechanisms (EX2 and EX1 mechanisms) for the three-state model of the H/D-exchange. In the EX2 mechanism, k_{close} is much larger than k_{int}, the opening and closing occurs repeatedly before the H/D exchange step, so that

$$(k_{close} + k_{int}) \cong k_{close} \qquad (1\text{-}6)$$

Therefore, from Equation (1-5), we have

$$k_{ex} = k_{open} \cdot k_{int} / k_{close} = (k_{open} / k_{close}) \cdot k_{int} = K_{open} \cdot k_{int} \quad (1\text{-}7)$$

The observed exchange rate constant k_{ex} is thus given by the intrinsic exchange rate (k_{int}) multiplied by the fraction of time that the amide proton is accessible for H/D-exchange (K_{open}). The opening equilibrium constant K_{open} is thus given by a ratio of the observed and intrinsic exchange rate constants as,

$$K_{open} = k_{ex} / k_{int} \quad (1\text{-}8)$$

The protection factor (P_f) of the amide proton against the H/D-exchange is defined as the inverse of K_{open}, and hence given by

$$P_f = k_{int} / k_{ex} \quad (1\text{-}9)$$

However, when $k_{close} \ll k_{int}$ the H/D-exchange takes place in every opening step with k_{int} (EX1 mechanism), so that

$$(k_{close} + k_{int}) \cong k_{int} \quad (1\text{-}10)$$

The observed exchange rate constant k_{ex} is thus given by

$$k_{ex} = k_{open}.k_{int} / k_{int} = k_{open} \quad (1\text{-}11)$$

In the EX1 mechanism, the overall exchange reaction is thus rate-limited by the structural opening step of the protein. The EX1 mechanism is usually observed at a highly alkaline pH, where k_{int} is very large, and at neutral and acidic pH region, the EX2 mechanism prevails in most globular proteins.

1.3.2. The H/D exchange and structural fluctuations

It has been widely studied and accepted that the H/D-exchange behavior of proteins depends on fluctuations in their structure. The exchangeable protons of proteins are distributed over the entire region, and they form structurally crucial hydrogen bonds in the α-helices, β-strands, and bends. Their exchange with solvent protons is known to respond to the binding of small and large molecules, to allosteric and other alterations, and to solution and environmental variables. Thus the H/D-exchange analysis provides useful information about the structural fluctuations at many sites along the polypeptide chains, their dependence on local structure and structural changes, and their interplay with biological functions.[45] As shown in Figure 1-6, the H/D-exchange reactions of a protein in the native state take place through (1) local fluctuation (2) partial unfolding, and (3) global unfolding of the protein molecule.[46, 47]

Local Fluctuations

There are many proteins which have local fluctuations in the solution. The most important factors for protection against the H/D-exchange are hydrogen bonding of amide protons and protection from solvent penetration in the interior of protein. The hydrogen exchange is mainly affected by protein mobility and structural flexibility, which break hydrogen bonds of amide groups that are exposed on the protein surface. Sometimes, amide protons that are highly buried or hydrogen bonded can be exchanged through structural fluctuations that allow transient exposure of the amide groups or transient solvent penetration. The small amplitude fluctuations which change solvent protected hydrogen to a solvent exposed hydrogen are completely reversible, these motions are described as the local fluctuations. A local unfolding can involve one or many amide groups of a protein and is result in simultaneous exposure of the amides to the solvent.[45]

Maity *et al*.[48] replaced a surface lysine residue (Lys8) in recombinant cytochrome *c* (cyt *c*) with glycine. The lysine to glycine mutation has no effect on the native protein structure, but it induced a large change on the protein stability, which allowed them to study the effect of local fluctuations on the protein H/D-exchange pattern.

In general, the amide protons which are on the surface of proteins are highly accessible to the solvent and are easy to exchange with the solvent deuterons, whereas the amide protons which are deeply buried in a core region of a protein are inaccessible and are slow to exchange. The observed exchange rate constant k_{ex} values of the amide protons exchanged by local fluctuations generally do not show any significant dependence on the concentration of a denaturant (urea or guanidinium chloride (GdmCl)).

Partial unfolding

In the partial unfolding, one or more domains of a protein remain folded, whereas the other domains are unfolded. By measuring the H/D-exchange kinetics of the peptide amide protons, which are identified by 2D NMR spectra and also by studying the dependence of the exchange kinetics of these amide protons on denaturant concentration, it is often possible to characterize the amide protons that are exchanged by partial unfolding, and to determine which portion of the protein exhibits transient partial unfolding under the native condition. The k_{ex} values of the amide protons exchanged by partial unfolding show significant dependence on denaturant concentration, but the slope of the ln k_{ex} vs. denaturant concentration plot is smaller than that for the amide protons exchanged by global unfolding. Over the years, amide H/D-exchange techniques have been developed which have allowed the characterization of a number of different partially folded states: heterogeneous equilibrium molten globule states; rare, partially

folded conformations in equilibrium with the native conformation; and transient intermediates in the kinetic folding process.

Wani *et al.*[49] studied folding of an SH3 domain by H/D-exchange techniques in the absence and in the presence of a denaturant (GdmCl). In the absence of the denaturant, unfolding occurs in two steps. In the first step, amide protons protected against the H/D-exchange lose their protection, and an intermediate is formed. In the second step, all amide hydrogen sites become unprotected during transient formation of the unfolded SH3 domain. In the presence of a 1.8 M of the denaturant, the unfolding reaction also occurs in the two steps, formation of the intermediate followed by unfolding of the SH3 domain with the same structural transition studied in the absence of the denaturant. Thus, the initial unfolding intermediate has the same structure in both conditions.

Arai *et al.*[50] studied formation of a molten globule intermediate in refolding of *α*-lactalbumin. In this study, they found that the burst-phase intermediate is characterized as a state that has substantial, hydrogen-bonded secondary structure and a hydrophobic surface highly exposed to solvent, but has no rigid side chain packing. Furthermore, the stability of the secondary structure in the burst-phase intermediate is identical with that in the equilibrium molten globule state. H/D-exchange studies on apomyoglobin also predict the formation of partly folded intermediate species.[51]

Global unfolding

If a protein is subjected to global unfolding, highly protected amide protons, which are stabilized by hydrogen bonding or deeply buried inside the protein becomes easily accessible to solvent for H/D-exchange. Even under a strongly native condition, proteins undergo transient

global unfolding, which can be detected by the H/D-exchange techniques, although the fraction of the globally unfolded species should be extremely small, often much less than a millionth. Under the EX2 condition, there are amide protons that exchange on a timescale ranging from days to months, and these protons exchange only when the protein is fully unfolded. From the k_{ex} value of the amide protons that are exchanged by global unfolding, we can estimate the effective thermodynamic stability (ΔG_{eff}), of the protein, and the ΔG_{eff} is related to K_{open} and $P_{f,}$[45] obtained by the H/D-exchange experiment, as

$$\Delta G_{eff} = -RT \ln K_{open} = RT \ln P_f \qquad (1\text{-}12)$$

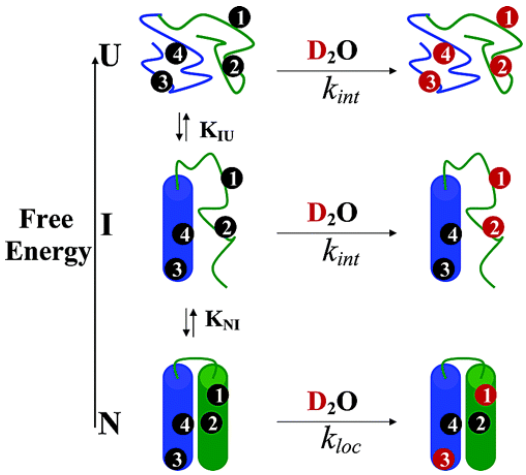

Figure 1-6. Illustration of three processes of hydrogen exchange for a protein with a partially unfolded intermediate: local fluctuation process (bottom); partial unfolding process (middle); and global unfolding (up). The figure was taken from Bai *et al* with permission.[47]

It is now well established that this relationship exists in many globular proteins that shows the H/D-exchange by global unfolding and that the ΔG_{eff} values are reasonably coincident with the Gibbs free-energy changes of equilibrium unfolding.

The relative importance of local, sub-global and global unfolding depends on experimental conditions, and at a physiological pH and temperature in the absence of denaturant, local unfolding may prevail, whereas at a high concentration of denaturant, the global unfolding becomes predominant. The k_{ex} values for the amide protons that are exchanged by global unfolding shows the strongest dependence on denaturant concentration, and as the denaturant concentration increases, the amides that are exchanged by local unfolding shift towards global unfolding. H/D-exchange experiments with cyt *c* have shown that some hydrogens in cyt *c* exchange with solvent by transient global unfolding, some through sub-global unfolding, and some through local fluctuations.[46, 52]

1.4. 2D NMR Spectroscopy

1.4.1. 2D HSQC

1D NMR spectra are plots of intensity vs. frequency, and in 2D NMR spectra, the intensity is plotted as a function of two frequencies, F_1 and F_2. 2D NMR spectroscopy allows data collection in two different time domains (t_1 and t_2); a successively incremented delay (t_1), called evolution period, elapses after an initial radio-frequency (RF) pulse before detection, and then the free-induction decay (FID) caused by another pulse (detection pulse) is acquired during t_2. In the HSQC spectroscopy, proton magnetization is transferred to other nuclei like those of ^{15}N and ^{13}C, and after the evolution period, the t_1 magnetization is returned back to the proton for observation. The 2D-HSQC spectrum provides correlations between amide protons and ^{15}N or ^{13}C nuclei

which are connected with the amide protons. Figure 1-7 shows typical two-dimensional [^{15}N,^{1}H]-correlation experiment; there are four steps for this experiment, i.e., preparation, evolution, mixing and detection. The preparation usually consists of a 90° pulse which excites sample nuclei. During the preparation period, protons thus get excited, creating magnetizations in the x-y plane. During the evolution period, the magnetizations produced by the preparation pulse show time evolutions with frequencies of individual protons with different chemical shifts. The mixing is a combination of RF pulses and/or pulse delay periods, leading to the transfer of magnetization from protons to ^{15}N or ^{13}C nuclei, and this process occurs via direct spin-spin couplings or spin-spin couplings occurring through space. The detection step involves recording the FID produced by the detection pulse and finding the frequency components of ^{15}N or ^{13}C nuclei by Fourier transformation. As a protein has the backbone amide groups, each amide group produces one peak in the spectra except prolines which lack an amide proton. HSQC can also be used in a triple resonance experiment, where each proton is correlated with ^{15}N and ^{13}C, leading to a clear non-overlapped spectra, and this has been used for assignment of individual amide proton peaks.[53, 54]

The recording of 2D NMR data set involves repeating a pulse sequence for increasing values of t_1 and recording of the FID as a function of t_2 for each value of t_1. The 2D NMR signal is thus recorded in the following way. First, with the t_1 value set to zero, the FID is recorded after executing the pulse sequence, and then the nuclear spins are allowed to return to equilibrium. Next, t_1 is set to Δt_1, the sampling interval in t_1, the pulse sequence is executed, and the FID is recorded and stored separately from the first FID. Again the spins are allowed to set at equilibrium, t_1 is set to $2\Delta t_1$, the pulse sequence is repeated, FID is recorded and stored separately. The whole procedure is repeated again for $3\Delta t_1$, $4\Delta t_1$, $5\Delta t_1$ and so on until sufficient data is recorded.

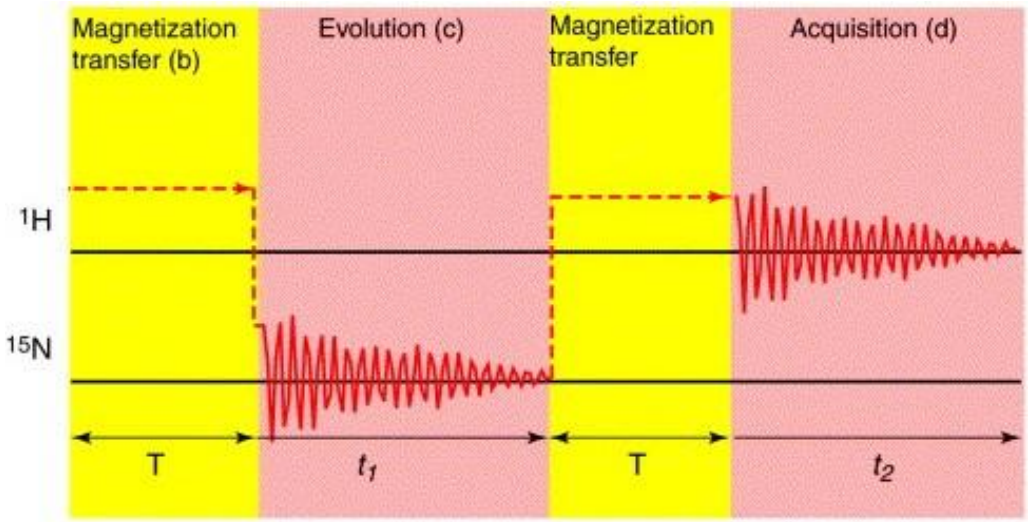

Figure 1-7. In a two-dimensional [^{15}N,^{1}H]-correlation experiment, one first creates proton magnetization. This is then transferred to ^{15}N via a polarization transfer element. After 'frequency labeling' of the ^{15}N magnetization during the evolution period, $\boldsymbol{t}_1$, magnetization is transferred back to ^{1}H via a reverse polarization transfer element and then detected on ^{1}H during the acquisition period, $\boldsymbol{t}_2$. The figure was taken from Riek *et al.* with permission.[55]

1.4.2. TROSY

The major problem for studies of biomolecules with a molecular weight larger than 10 kDa is the fast decay of NMR signal due to relaxation. There are two main reasons for the size limit of less than 10 kDa: (1) Spectral crowding due to a large number of overlapping signals, which affects spectral resolution, and (2) NMR signals of a large molecule relax faster due to the fast transverse relaxation rates ($1/T_2$) of nuclei, which ultimately results in the poor resolution and loss of signals due to line broadening. The line width in NMR spectra is inversely proportional to the relaxation rate, which depends on the size of the molecule; therefore, for a large protein with

a molecular weight larger than 10 kDa, the relaxation time T_2 is very short, and the signal to noise ratio is very poor, leading to collapse of spectral recording.

Two major factors contributing line broadening of proton signals in the $^{1}H–^{15}N$ HSQC spectra are (1) dipole-dipole (DD) interactions between proton and ^{15}N spins and (2) chemical shift anisotrophy (CSA) of protons. Any magnetic nucleus in a molecule generates an instantaneous magnetic dipolar field that is proportional to the magnetic moment of the nucleus. As the molecules tumble in solution, this field fluctuates and constitutes a mechanism for relaxation of nearby spins. For proteins, the main source of the relaxation by the DD interactions is nearby protons and protons attached to ^{15}N. In TROSY, a protein sample used is thus perdeuterated to suppress these DD interactions. The CSA of protons depends on the orientation of the molecule, as nuclei can have a different magnetic field, depending on the orientations with respect to the applied bulk magnetic field. The CSA increases with increasing the external magnetic field, whereas the DD interactions are independent of the static magnetic field. Chemical shifts reflect the electronic environments that modify the local magnetic fields experienced by different nuclei, and these local fields are anisotrophic. Therefore, the components of local fields vary as the molecule reorients due to molecular motion, contributing as a source of relaxation. TROSY reduces the line broadening and hence the fast decay of the magnetization by recording only the smallest relaxation component of splitted multiplet signals of a nucleus.

TROSY thus exploits constructive interference between the DD-coupling and the CSA and reduce the transverse relaxation rates during the frequency labeling period and acquisition. In ^{1}H-^{15}N- HSQC, the NMR signals of each nucleus have spin up and spin down positions relative to the external magnetic field, and it splits into two components due to spin-spin coupling, leading to the formation of four peaks. These four peaks are collapsed into a single centrally located peak

using decoupling, and such a single peak has an average chemical shift of the four components. However, these four individual peaks have different transverse relaxation rates, leading to the different line-width lines, which are mixed by decoupling, and in case of a large molecular structure studied at high magnetic fields, the line broadening of the individual multiplet components is very much pronounced, resulting in deterioration of the average central peak signal.

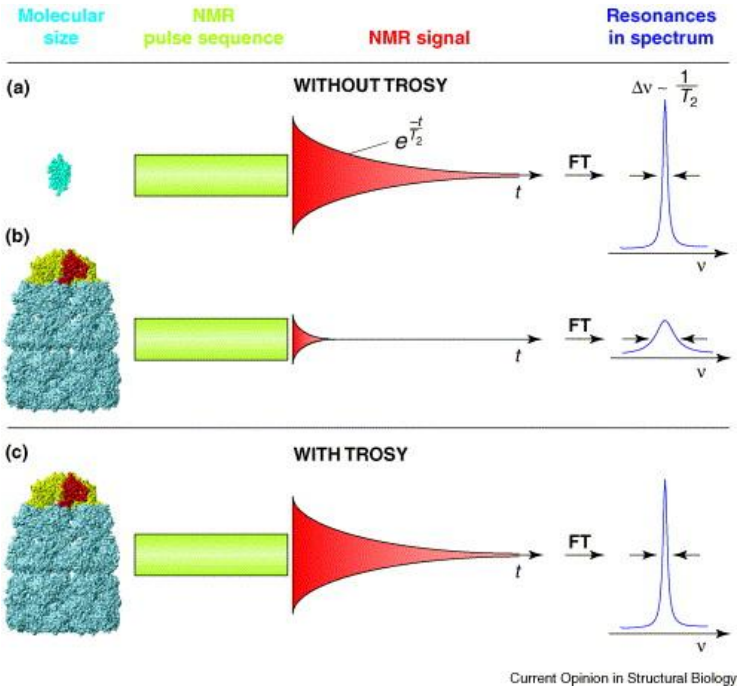

Figure 1-8. NMR spectroscopy with small and large molecules in solution. (a) The NMR signal obtained from small molecules in solution relaxes slowly; it has a long transverse relaxation time (T_2). A large T_2 value translates into narrow line widths ($\Delta\nu$) in the NMR spectrum after Fourier transformation (FT) of the NMR signal. (b) By contrast, for larger molecules, the decay of the NMR signal is faster (T_2 is smaller). This results both in a weaker signal measured after the NMR pulse sequence and in broad lines in the spectra. (c) Using TROSY, the transverse relaxation can be substantially reduced, which results in improved spectral resolution and improved sensitivity for large molecules. The figure was taken from Fernandez *et al.* with permission.[56]

In TROSY, these multiplet peaks are not decoupled, it records only the narrowest, most slowly relaxing component of each multiplet, which is independent of the transverse relaxation rate.[55,56] Figure 1-8 shows the NMR spectroscopy with small and large molecules in solution and the benefits of using TROSY for large molecules.

1.5. Scope of this study

To study the H/D-exchange mechanisms of protein supermolecular complexes, GroES and the GroES portion of the GroEL/GroES complexs, the direct H/D-exchange measurements by conventional 2D NMR spectra are not effective, and I used DMSO-QHX technique. Therefore, I first developed a new technique to carry out the DMSO-QHX analysis. Earlier studies since the inception of the DMSO-QHX methods, lyophilization has been used to remove D_2O from the protein solution, and later H/D-exchange reaction was quenched by using a DMSO solution as a solvent. As there is possibility of salt contamination after lyophilization, the amide H/D-exchange measurement may suffer from effective error. I thus developed a new technique for the medium exchange from D_2O to the DMSO solution by using Zeba spin desalting columns.[57] The medium exchange by using a Zeba spin column took only about ten minutes as compared with the overnight duration of lyophilization. I successfully mapped amide exchange kinetics of ^{15}N labeled ubiquitin by this technique. The results are described and discussed in Chapter 2.

After this small study, I started my new project in which I studied H/D-exchange kinetics of a large protein complex, i.e., free heptameric GroES. To fully understand biological functions of the chaperonin GroEL/GroES complex, it is necessary to study structural fluctuations of free GroES and the GroES portion of the GroEL/GroES complexes under different nucleotide conditions. Thus, in the present thesis, I further applied the H/D-exchange and 2D NMR

techniques to study free heptameric GroES. However, as the molecular weight of the GroES complex is 73 kDa, I couldn't obtain good NMR spectra. Therefore, I used TROSY for direct H/D-exchange measurements of perdeuterated GroES and also the DMSO-QHX technique with spin desalting columns. The results of these H/D-exchange measurements are described and discussed in Chapter 3.

In Chapter 4, I summarize the present study and discuss future perspectives. I also describe preliminary results of the H/D-exchange kinetics of the GroES portion of the SR1/GroES complex in the presence of ADP; SR1 is a single-ring mutant of GroEL.

Thus, the study in my thesis overall solves the mystery of dynamic fluctuations of the GroES part from the GroES-GroEL chaperonin complex.

Chapter 2. The use of spin desalting columns in DMSO-quenched H/D-exchange NMR experiments

This chapter is adapted and modified from Mahesh S. Chandak, Takashi Nakamura, Toshio Takenaka, Tapan K. Chaudhuri, Maho Yagi-Utsumi, Jin Chen, Koichi Kato and Kunihiro Kuwajima, The use of spin desalting columns in DMSO-quenched H/D-exchange NMR experiments. *Protein Sci.* 2013, **22**(4):486-91

2.1. Introduction

The DMSO-QHX method, first introduced by Zhang *et al*.,[58] is a very versatile method to characterize the H/D-exchange behaviors of proteins and protein assemblies, and the advantage of this method is two-fold. First, DMSO is a strong protein denaturant that can be used as a solubilizer of water-insoluble protein aggregates. Second, the chemical exchange rates of peptide amide protons are substantially reduced in a DMSO solution (most typically 95% DMSO-d_6/5% D_2O, pH* 5.0), making it possible in principle to observe the H/D-exchange of non-protected fast-exchanging amide protons by 2D NMR spectroscopy; pH* indicates the pH-meter reading. The DMSO-QHX method has thus been used widely for studying the H/D-exchange behaviors of various amyloid fibrils[40, 59-65] and other protein supermolecular assemblies.[66, 67] The method has also been used for studying the H/D-exchange of non-protected fast-exchanging amide protons in the intermediate and the unfolded states of proteins.[58, 68-70]

In the DMSO-QHX experiments, the H/D-exchange reactions are first carried out in a D_2O buffer solution under a condition used to investigate the exchange behavior of a protein. After a pre-determined exchange time, the exchange reaction is quenched in liquid nitrogen, and the medium is changed from D_2O to the DMSO solution, in which amyloid fibrils or other insoluble protein aggregates are dissolved into monomers. When protein is ^{15}N-labeled, we can use 2D ^{1}H–^{15}N HSQC spectra to monitor the individual amide-proton signals of the protein with different exchange times, because further exchange is effectively quenched in the DMSO solution.

However, in all of the previous DMSO-QHX studies of proteins so far reported, lyophilization was used to remove D_2O from the protein solution, and the lyophilized protein was dissolved in the DMSO solution.[40, 58-70] Therefore, the current DMSO-QHX method has not

been used for studies on fully unfolded proteins in a concentrated denaturant (6 M GdmCl or 8 M urea) or protein solutions at high salt concentrations because the denaturants or salts remain after lyophilization, although the DMSO-QHX method is potentially useful for investigating non-protected fast-exchanging amide protons in the unfolded state.

In this chapter, I report that the use of spin desalting column is a very effective alternative to lyophilization for the medium exchange from the D_2O buffer to the DMSO solution in the DMSO-QHX experiments. I thus, report that the medium exchange by a spin desalting column takes only about 10 min in contrast to an overnight length of time required for lyophilization, and that the use of spin desalting columns has made it possible to monitor the H/D-exchange behavior of a fully unfolded protein in a concentrated denaturant. In this chapter, I report the results of unfolded ubiquitin in 6.0 M GdmCl.

2.2. Results and discussion

I used Zeba^{TM} Spin Desalting Columns (Thermo Scientific, Rockford, IL, USA) for the medium exchange and 95% DMSO-d_6/5% D_2O (pH* 5.0) as the DMSO solution to quench the H/D-exchange. When I used the spin desalting column for the medium exchange, the column was first filled with the DMSO solution, and an appropriate volume of a sample protein solution in the D_2O buffer was applied to the column. To investigate the most appropriate volume of the sample, I applied different volumes of 50 mM phosphate buffer in H_2O (pH 7.0) to a column filled with the DMSO solution, and measured 1D ^{1}H-NMR spectra of the eluates. For a 5-mL spin desalting column, the manufacturer's recommended applied volume is 0.5–2.0 mL.

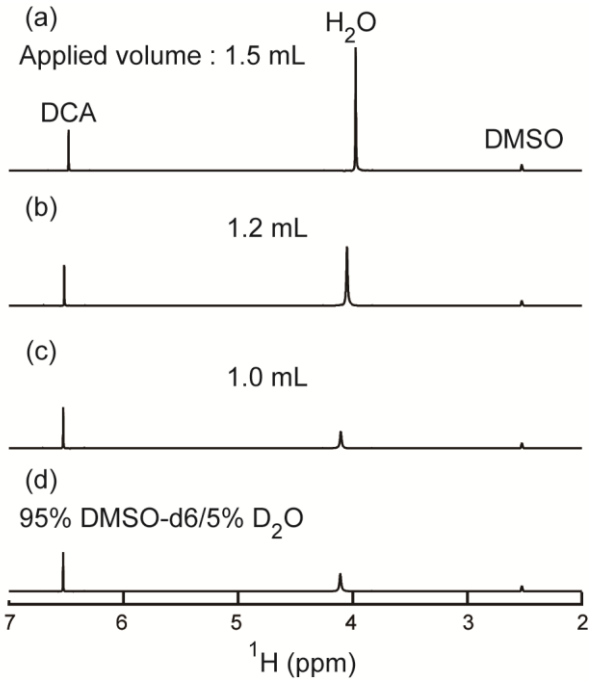

Figure 2-1. The 1D ^{1}H-NMR spectra of the elutes from the DMSO solution-filled spin columns when different volumes of 50 mM phosphate buffer in H_2O (pH 7.0) were applied to the column. The applied volumes were (a) 1.5 mL, (b) 1.2 mL, and (c) 1.0 mL. The 1D ^{1}H-NMR spectrum of the DMSO solution (95% DMSO-d_6/5% D_2O, pH 5.0) is also shown in (d). NMR peaks for H_2O, DCA, and DMSO are shown in the figure.

As shown in Figure 2-1, however, I observed a significant water contamination when I applied more than 1.0 mL of solution, and hence I determined the best application volume to be 1.0 mL. For a 2-mL spin desalting column, the best application volume was found to be 0.35 mL.

I used ^{15}N-labeled ubiquitin as a model protein to examine the application of spin desalting columns in the DMSO-QHX 2D NMR (^{1}H–^{15}N HSQC) studies; the ubiquitin used in the present study contained an extra 34 residues at the N-terminus (see Materials and Methods) as compared to wild type ubiqutin. The H/D-exchange reaction of unfolded ubiquitin was started by 10-fold

dilution of 3 mM ^{15}N-labeled ubiquitin unfolded in 6.0 M GdmCl (H_2O) at pH 2.6 into 6.0 M deuterated GdmCl in D_2O at pH* 2.6 and 20.0°C. At each pre-determined exchange time, 1.0 mL of the reaction mixture pre-dispensed in a microtube was taken, the reaction was quenched in liquid nitrogen, and the frozen mixture was kept in a freezer at −85°C until the medium exchange and the subsequent NMR measurement. For the NMR measurement, the frozen sample was thawed at room temperature, the medium containing 6.0 M GdmCl was exchanged for the DMSO solution by using a spin desalting column, and the ^{1}H–^{15}N HSQC spectrum of the protein was measured. The medium exchange by the spin desalting column took only about 10 minutes, which is thus a big advantage over the overnight lyophilization that has been used in the conventional DMSO-QHX method.

Figure 2-2 shows the HSQC spectra of ubiquitin obtained using different exchange times of 0, 10, and 60 min (panels (a), (b), and (c)), and the spectrum after complete H/D-exchange by heating at 55°C for 30 min ((d)); the exchange times shown are the exchange times under the H/D-exchange condition, not including the time required for the medium exchange, and the heating was done in 6.0 M GdmCl at pH* 2.6 (90% D_2O/10% H_2O).

The amide proton signals were well resolved, and the quality of the spectra was identical to that of the spectrum of the sample solution obtained by direct dissolution of lyophilized ubiquitin in the DMSO solution. In recent DMSO-QHX NMR studies, pure DMSO-d_6 (or 99% DMSO-d_6/1% trifluoroacetic acid) was used as a quenching medium instead of the DMSO solution (95% DMSO-d_6/5% D_2O, pH* 5.0).[61, 66, 67] The spin desalting column could also be used for the medium exchange for pure DMSO, and hence I prepared the ubiquitin sample in pure DMSO-d_6 and measured its HSQC spectrum (data not shown). However, the spectrum was collapsed, and its quality was worse than the spectral quality in the DMSO solution in the case of ubiquitin.

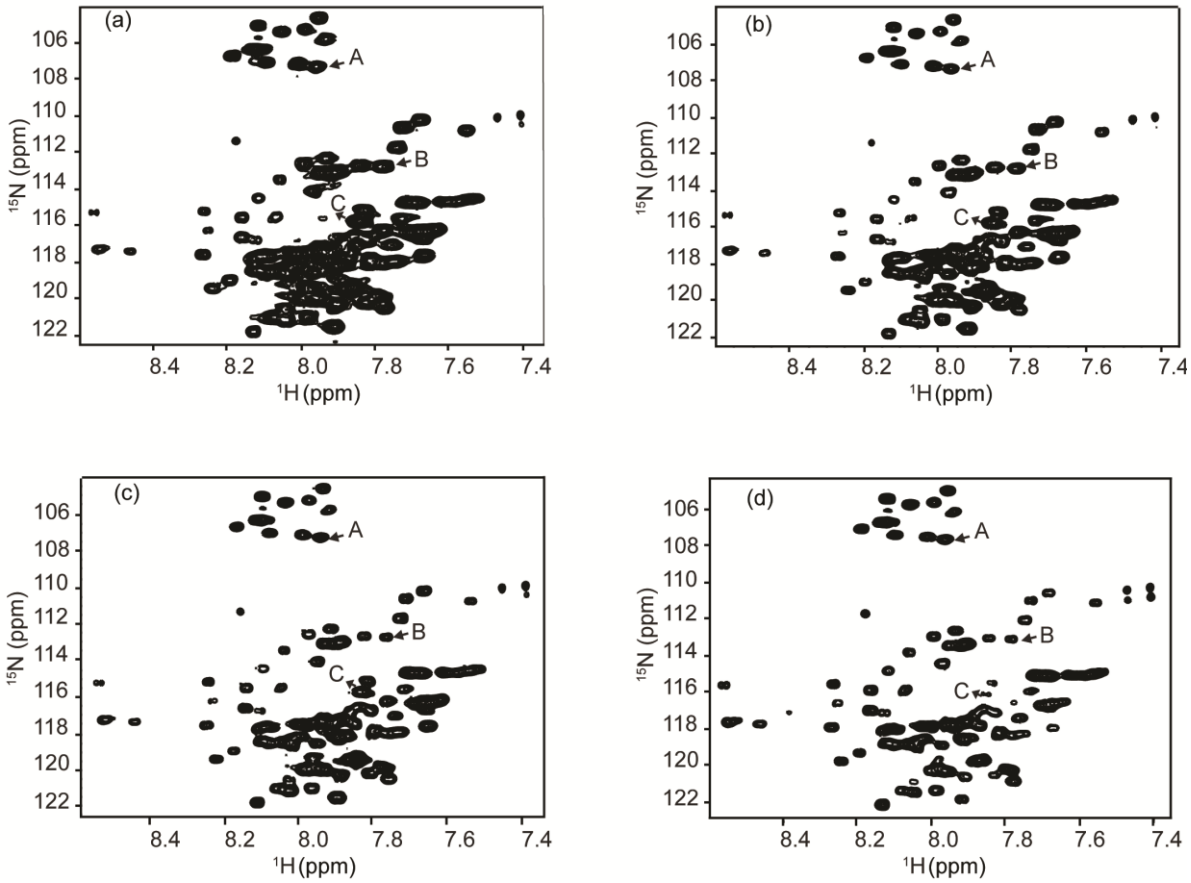

Figure 2-2. ^{1}H–^{15}N HSQC spectra of ^{15}N-labeled ubiquitin in the DMSO solution with different exchange times under the H/D-exchange conditions (90% D_2O/10% H_2O, 6.0M GdmCl, pH* 2.6, and 20.0°C): (a) The unexchanged sample, (b) 10 min, (c) 60 min, and (d) after complete exchange by heat treatment at 55°C for 30 min.

Figure 2-3 shows typical H/D-exchange curves of three amide proton resonances labeled "A," "B" and "C" in Figure 2-2, I calculated the predicted half times of the H/D-exchange for the non-protected amide protons in the whole sequence of the protein under the present exchange conditions (pH* 2.6 and 20°C),[43,44] and they ranged from 1.5 to 19 min except for the amide proton of the second amino acid residue in the sequence, which had a predicted half time of 0.7 min.

Loftus *et al*.[71] previously reported that the presence of 6.0 M GdmCl resulted in a two-fold deceleration of the H/D-exchange rate of the peptide amide groups, and hence the predicted half times ranged from 3.0 to 38 min. Amide proton A may belong to a glycine residue according to its chemical shift values. Because the H/D-exchange rate of the glycine residue was relatively fast in the DMSO solution, a significant portion of the amide proton signal was lost during the NMR measurement, but nevertheless, I observed a single-exponential decay of the signal with a half time of 18 min (Figure 2-3(a)), which was within the range of the predicted exchange half times. Amide proton B showed a stronger signal with a half time of 16 min (Figure 2-3(b)), which was also within the range of the predicted exchange half times for the non-protected amide protons. Amide proton C, which showed an even stronger signal, however, was exchanged much more slowly, with a half time of 117 min, which was at least three times longer than the predicted half times for the non-protected protons. Among the 12 additional amide protons for which I analyzed the H/D-exchange kinetics, three showed a half time longer than 90 min. Ubiquitin was shown to be fully unfolded at 6.0 M GdmCl at pH 2–3.[72] It thus remains to be determined whether the amide protons that showed an exchange half time longer than 90 min arose from a weakly protected portion of a locally structured region in the unfolded protein or rather from a slight inaccuracy in the predicted exchange rates.

Finally, I also investigated whether or not, the present method is equally applicable to a protein dissolved in DMSO, because DMSO is often used as a solubilizer of insoluble protein aggregates such as amyloid fibrils.[40] For this purpose, I dissolved lyophilized powder of ^{15}N-labeled ubiquitin in 100% DMSO, exchanged the medium (100% DMSO) for the DMSO solution by a spin desalting column, and measured the ^{1}H–^{15}N HSQC spectrum of the eluate. The spectrum thus obtained was identical to that shown in Figure 2-2(a), indicating that the present method is not only useful for water-soluble proteins but also for insoluble protein aggregates that can be dissolved in DMSO.

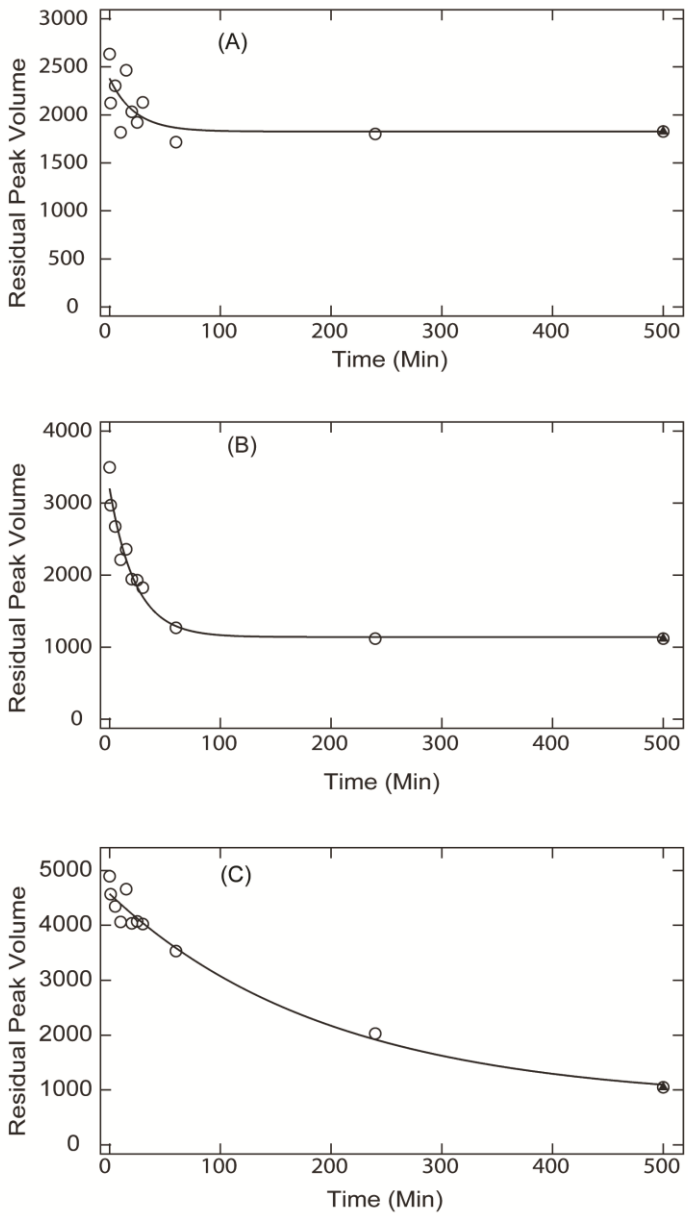

Figure 2-3. The kinetic progress curves of H/D-exchanged ^{15}N-labeled ubiquitin in 6.0 M GdmCl at pH* 2.6 and 20.0°C (open circles). Panels (A), (B), and (C) represent the kinetic progress curves for H/D-exchange of amide protons corresponding to signals A, B and C, respectively, shown in Figure 2-2. The filled triangle in each panel represents the sample after complete exchange by heating at 55°C for 30 min.

In conclusion, the use of spin desalting columns in the DMSO-QHX studies of proteins was very effective, and allowed us to successfully obtain the H/D-exchange kinetics of the individual amide protons, H/D-exchange-quenched by DMSO and detected by $^{1}H–^{15}N$ HSQC spectroscopy, of unfolded ubiquitin in 6.0 M GdmCl, which was previously impossible by using the conventional DMSO-QHX technique with lyophilization for the medium exchange. Because the medium exchange by a spin desalting column is relatively easy to handle and takes a much shorter time than lyophilization, the use of spin desalting columns is superior to lyophilization, and will be more widely employed in future DMSO-QHX studies.

2.3. Materials and Methods

2.3.1. Chemicals

DMSO-d_6 and D_2O were purchased from Cambridge Isotope Laboratories Inc. (Andover, MA,USA). Dichloroacetic acid (DCA) was purchased from Tokyo Chemical Industry Co., Ltd. (Tokyo, Japan). GdmCl was purchased from Nakalai Tesque Inc. (Kyoto, Japan). Deuterated GdmCl was produced by repeated cycles of dissolution of GdmCl in D_2O followed by lyophilization.

2.3.2. ^{15}N-Labeled ubiquitin

Human ubiquitin was bacterially expressed as a recombinant protein and purified as described in the literature[73] with slight modifications. The plasmid vector was constructed and cloned using the pET28a(+) vector (Novagene, Madison, WI, USA), then transformed into *E. coli* strain BL21-CodonPlus (Stratagene, La Jolla, CA, USA). For the production of isotopically

labeled ubiquitin, cells were grown in M9 minimal media containing [^{15}N]NH_4Cl (1 g/L). Ubiquitin thus expressed was flanked by an N-terminal hexahistidine-tag moiety, MGSSHHHHHHSSGLVPRGSHMASMTGGQQMGRGS, and a C-terminal amyloid β segment. After purification by a Ni^{2+}-nitrilotriacetic acid affinity column (GE Healthcare, Buckinghamshire, UK), ubiquitin was enzymatically cleaved from the C-terminal amyloid β segment. Ubiquitin with the N-terminal extension was further purified by reverse-phase chromatography using an octylsilane column (Sunniest C8; ChromaNik, Osaka, Japan) with a linear gradient of acetonitrile. The fraction containing ubiquitin was collected and lyophilized.

2.3.3. DMSO-QHX experiments

The H/D-exchange reaction of unfolded ubiquitin was started by 10-fold dilution of 3 mM ^{15}N-labeled ubiquitin unfolded in 6.0 M GdmCl (H_2O) at pH 2.6 into 6.0 M deuterated GdmCl in D_2O at pH* 2.6 and 20.0°C. Immediately after the dilution, 1.0 mL of the reaction mixture was dispensed into each of 10–20 microtubes with a screw cap sealed by an O-ring to prevent water contamination, and the solutions in the tubes were incubated at 20.0°C for H/D-exchange. At each pre-determined exchange time between 5 and 240 min, the reaction mixture in a tube was taken, and the reaction was quenched in liquid nitrogen. The frozen mixtures were kept in a freezer at −85°C until the medium exchange and the subsequent NMR measurement.

For the medium exchange for the DMSO solution (95% DMSO-d_6/5% D_2O, pH* 5.0), I first removed the storage solution from a spin desalting column (Zeba^{TM} Spin Desalting Column 89891, 5 mL; Thermo Scientific) by centrifuging the column at 1000 × *g* for 2 min. I then added 2.5 mL of the DMSO solution to the column, and centrifuged the column at 1000 × *g* for 2 min to remove the excess DMSO solution. This process was repeated two or three additional times to fill the column with the DMSO solution. Before sample loading on the spin column, the frozen

reaction mixture was thawed at room temperature, and the sample solution thus obtained was slowly applied to the center of the compact resin bed of the column. The sample in the DMSO solution was collected by centrifuging the column at 1000 × *g* for 2 min, and immediately subjected to NMR measurement to detect the amide proton signals of the protein.

2.3.4. NMR measurements

All NMR spectra were acquired at 25°C on a Bruker Avance 500 spectrometer. The standard $^{1}H–^{15}N$ HSQC experiment was carried out on ^{15}N-labeled ubiquitin in the DMSO solution. The ^{1}H chemical shifts were directly referenced to the resonance of tetramethylsilane, while the ^{15}N chemical shifts were indirectly referenced with the ratio of the ^{15}N and ^{1}H chemical shifts.[74] All NMR data were processed using NMRPipe[75] and NMRView.[76]

2.3.5. Data analysis

The NMR signal intensities of the amide protons observed by the $^{1}H–^{15}N$ HSQC spectra of the protein showed single-exponential decay curves with respect to the exchange time under the H/D-exchange condition (6.0 M GdmCl, 90% D_2O/10% H_2O and pH* 2.6 at 20.0°C) (Figure 2-3). The exchange half times $t_{1/2}$ of the amide protons were given by $t_{1/2} = (\ln 2)/k_{ex}$, where k_{ex} represents the observed rate constants of the H/D-exchange reactions. The predicted half times of the H/D exchange for the non-protected amide protons were calculated by the methods of Bai *et al*.,[43] and Connelly *et al*.[44] We used the program SPHERE for the calculation of the predicted half times; SPHERE is accessible through the internet at the following URL, http://www.fccc.edu/research/labs/roder/sphere/sphere.html.

The observed kinetic exchange curves, given by the volumes ($Y(t)$) of cross peaks in 2D NMR spectra as a function of the H/D-exchange time (t), were single exponential fitted to the equation

$$Y(t) = A \cdot e^{-k_{ex}t} + Y_{\infty} \qquad (2\text{-}1)$$

where A and Y_{∞} are the kinetic amplitude and the final value of the peak volume, respectively. The fitting was performed by the IGOR Pro 6.2 software package (WaveMetrics).

As the H/D-exchange reaction was started by 10-fold dilution of the protein in H_2O into the D_2O solvent, ideally the final peak volume (Y_{∞}) should come down to the 10% of the initial peak volume. However, in the DMSO-QHX method, the NMR spectra were measured in the DMSO solution (95% DMSO-d_6/5% D_2O, pH* 5.0), and the H/D exchange was not completely quenched in the DMSO solution. Therefore, the Y_{∞} value depended not only on the H/D-exchange condition (90% D_2O/10% H_2O) but also on how much H/D exchange took place in the DMSO solution during the NMR measurement. When there is H_2O contamination in the DMSO solution, there must be a significant back exchange from the deuterated amide ND to NH. For example, if there is 1% H_2O contamination, it may result in 20% proton occupancy after full exchange, because 95% of the DMSO solution (i.e., 95% DMSO-d_6) did not have exchangeable protons. Similarly, 2% H_2O contamination may result in 40% proton occupancy. To obtain the accurate Y_{∞} value, I thus prepared the sample after complete exchange under the H/D-exchange condition (90% D_2O/10% H_2O), and took the NMR spectrum of the sample in the DMSO solution.

Chapter 3. The H/D-exchange kinetics of the *Escherichia coli* co-chaperonin GroES studied by 2D NMR and DMSO-quenched exchange methods

This chapter is adapted and modified from Mahesh S. Chandak,Takashi Nakamura, Koki Makabe, Toshio Takenaka, Atsushi Mukaiyama, Tapan K. Chaudhuri, Koichi Kato and Kunihiro Kuwajima, The H/D-Exchange Kinetics of the Escherichia coli Co-Chaperonin GroES Studied by 2D NMR and DMSO-Quenched Exchange Methods. *J. Mol. Biol*. 2013, 425, 2541-60.

3.1. Introduction

The *E. coli* co-chaperonin GroES, which is a heptameric protein supermolecular assembly with a molecular weight of 73,000 forms a chaperonin complex with GroEL that is a tetradecameric protein assembly with a molecular weight of 800,000.[77-79] The chaperonin complex is a dynamic molecular machine that mediates the folding reactions of various proteins in the bacterial cell in an ATP-dependent manner. Although a large number of biophysical and biochemical studies on the molecular mechanisms of the chaperonin function have been reported,[27, 77-96] rather little is known about dynamic aspects and structural fluctuations of GroES, GroEL and the related complexes. Structural fluctuations of GroES and GroEL are definitely important for formation of the chaperonin complex, recognition of substrate proteins by the complex, and chaperonin cycling of the GroEL/GroES complex.[39, 97-104] The large molecular weights of GroES, GroEL and the chaperonin complex make it infeasible to study the structural fluctuations of these protein supermolecular assemblies by a H/D-exchange technique combined with conventional 2D NMR spectroscopy. Therefore, there were no H/D-exchange studies of these protein assemblies in the native state until, in a very recent report, Zhang *et al*. described nucleotide-induced conformational changes of GroEL mapped by H/D-exchange monitored by Fourier transform ion cyclotron resonance mass spectrometry combined with limited proteolysis and HPLC analysis, a technique useful for studying large proteins.[105]

For GroES, however, the monomeric molecular weight is only 10,000, and hence, we can employ the following two techniques to obtain the well-resolved NMR spectra required for the H/D-exchange measurements of individual amide protons: (1) 2D ^{1}H–^{15}N TROSY[56, 106] and (2) the DMSO-QHX method combined with the ^{1}H–^{15}N HSQC spectroscopy.[40, 58] The TROSY technique, in combination with perdeuteration of protein, has opened avenues to the study of

large proteins and protein assemblies with molecular weights larger than 50,000 by solution NMR,[56, 106] and the technique was successfully applied for the NMR analysis of GroES and the GroEL/GroES complex, in which only the GroES portion was uniformly ^{15}N-labeled.[20, 107] The DMSO-QHX method, first introduced by the Roder group,[58] was recently improved by Chandak *et al*,[57] by the use of spin desalting columns for medium exchange from D_2O to the DMSO solution (Chapter 2 of this thesis), and this improved method was used here.

The X-ray crystallographic structures of heptameric GroES and the GroEL/GroES/nucleotide complexes have been reported,[12, 19, 101, 108] and the protein data bank (PDB) coordinates are available for the complexes (PDB codes: 1AON, 1PCQ, 1PF9, 1SVT and 1SX4). The structure of each subunit of GroES is composed of an irregular β-barrel formed by 5 β-strands (strands B, C, D, E and F), several reverse turns, a short 3_{10}-helix (residues 87–91), the N- and C-terminal β -strands (strands A and G) located at the subunit-subunit interface, and two loop regions, a flexible mobile loop (residues 17–34) and a roof hairpin loop (residues 44–58) (Figure 3-1). The mobile loop of stand-alone GroES is natively unfolded as indicated by 1D and 2D NMR spectra and the reported crystal structure of GroES in which the mobile loop segment was disordered in six out of the seven subunits.[19, 97] The flexible nature of the mobile loop is crucial for the recognition by GroEL,[97-100] and the loop becomes structured upon interacting with GroEL.[12] Except for the mobile loop region, the GroES structure of the GroEL/GroES complexes is very similar to the structure of stand-alone GroES.[12] In spite of these unique structural characteristics of GroES, the unfolding transitions of GroES induced by denaturants and by increasing temperature are fully reversible,[109-114] and often interpreted in terms of a simple two-state model of the unfolding accompanied by dissociation from the heptameric native state to the monomeric unfolded state.

Here, I studied the H/D-exchange reactions of free heptameric GroES by the TROSY technique and the DMSO-QHX technique combined with 2D ^{1}H–^{15}N HSQC spectra measured at

a ^{1}H resonance frequency of 920 MHz. I quantitatively evaluated the apparent rate constants (k_{ex}) of H/D-exchange for 33 out of the 94 peptide amide protons of GroES and their protection factors (P_f), and for the remaining 61 residues, I obtained the lower and the upper limits of the k_{ex} and P_f values, respectively. I show that the P_f values (10^6–10^7) of the most highly protected amide protons are comparable in magnitude to those observed in typical small globular proteins but that the number of the highly protected amide protons ($P_f > 10^6$) are significantly smaller than those reported for the small globular proteins, indicating that significant portions of GroES are flexible and natively unfolded. The flexible regions with weakly-protected amide protons ($P_f < 10^4$) were mostly located in the mobile loop of residues 17–34, a reverse turn 49–52 at the top of the roof hairpin, and the region (strand E and the adjacent turns) between strands D and F (Figure 3-1). Considering the oligomeric nature and physiological concentrations (~35 μM in monomer units)[115-117] of GroES and the P_f values of the most highly protected amide protons, the effective thermodynamic stability of GroES is well designed so as to be comparable to the stability of the small globular proteins.

The P_f values of the most highly protected amide protons were, however, a few orders of magnitude larger than those expected from the equilibrium unfolding parameters previously reported, strongly suggesting that the equilibrium unfolding of GroES is more complicated than a simple two-state or three-state mechanism, and may involve more than a single intermediate.

3.2. Results

3.2.1. NMR spectra of GroES

The molecular weight (M_w = 73,000) of a free GroES heptamer is too large to obtain well-resolved NMR signals in conventional ^{1}H–^{15}N HSQC spectra of the protein. Figure 3-2(a) shows

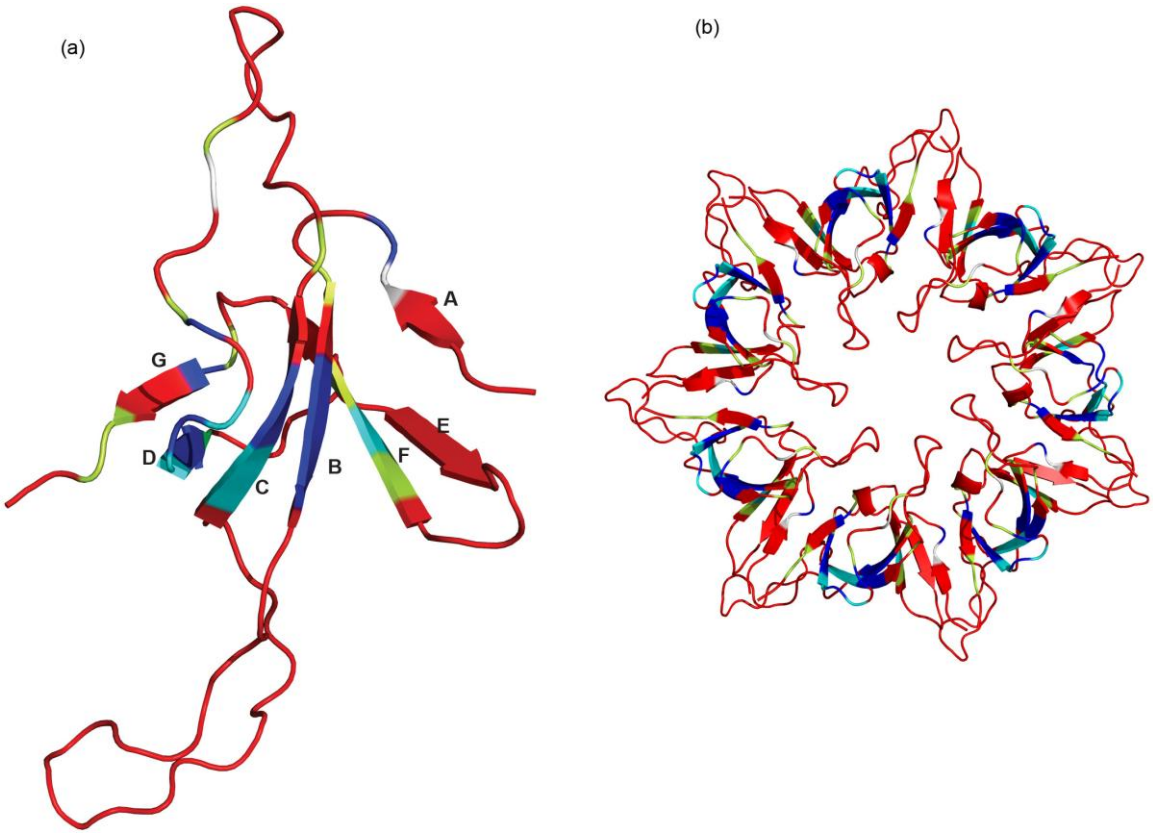

Figure 3-1. The backbone structure of the GroES monomer unit (a) and the heptameric complex (b). The GroES portion of the GroEL/GroES/ADP complex (PDB code: 1AON) is shown. The backbone structure was analyzed by the method of Kabsch and Sander[118] using the DSSP program (http://swift.cmbi.ru.nl/gv/dssp/). The seven β-strands thus identified are labeled as A, B, C, D, E, F, and G in the order from the N-terminal to the C-terminal side in (a). The structure is classified by different colors according to the P_f values (red for $P_f < 10^4$, yellow for $10^4 \leq P_f < 10^5$, cyan for $10^5 \leq P_f < 10^6$, and blue for $10^6 \leq P_f$). The residues for which only the upper limits of P_f are known (sticks and plus marks in Figure 3-8) are also shown in red. Two prolyl residues, Pro5 and Pro56, are shown in white. The figures were prepared using PyMOL (DeLano Scientific).

an HSQC spectrum of uniformly ^{15}N-labeled GroES in 90% H_2O/10% D_2O at pH 6.5 and 25°C; as shown in the figure, I observed only 20 out of 94 expected peptide amide ^{1}H–^{15}N cross peaks,

with the observed cross peaks belonging to the residue (Ala97) at the C terminus, residue 51 (Asn), and residues 17–34, which form a flexible mobile loop in the native state.[19, 97] To overcome the problem of these poor NMR signals, I employed two different techniques, i.e., (1) 2D $^{1}H–^{15}N$ TROSY[56, 106] at a ^{1}H resonance frequency of 920 MHz and (2) the DMSO-QHX technique combined with conventional $^{1}H–^{15}N$ HSQC spectroscopy.[57, 58] Although the long recording time (~2.5 h) required in the TROSY experiment precludes measurements of fast-exchanging amide-proton signals by TROSY, I could use the assignments of the amide-proton signals of GroES, previously reported by Fiaux *et al* (BMRB Entry 7091).[20] Figure 3-2(b) shows a TROSY spectrum of ^{15}N-labeled and perdeuterated GroES in 90% H_2O/10% D_2O at pH 6.5 and 25°C. I observed essentially all peptide-amide cross peaks of GroES, and the assignments for the 89 cross peaks previously reported are shown in Figure 3-2(b). The DMSO-QHX method is useful for measurements of the H/D-exchange kinetics of a protein supermolecular assembly, and the DMSO solution (95% DMSO-d_6/5% D_2O, pH* 5.0), which is used to quench the H/D-exchange reactions, effectively dissociates the GroES heptamer to unfolded monomers, making it possible to obtain well-resolved HSQC spectra of unfolded monomeric GroES.

However, we have to assign the HSQC cross peaks of GroES in the DMSO solution. The backbone assignments of {^{13}C, ^{15}N}-double labeled GroES in the DMSO solution were thus obtained by 3D CBCACONH and HNCACB experiments recorded on a 920-MHz NMR instrument. I obtained assignments of 46 out of the 94 backbone amide protons, and Figure 3-2(c) shows a $^{1}H–^{15}N$ HSQC spectrum of GroES in the DMSO solution (Figure 3-2(c)).

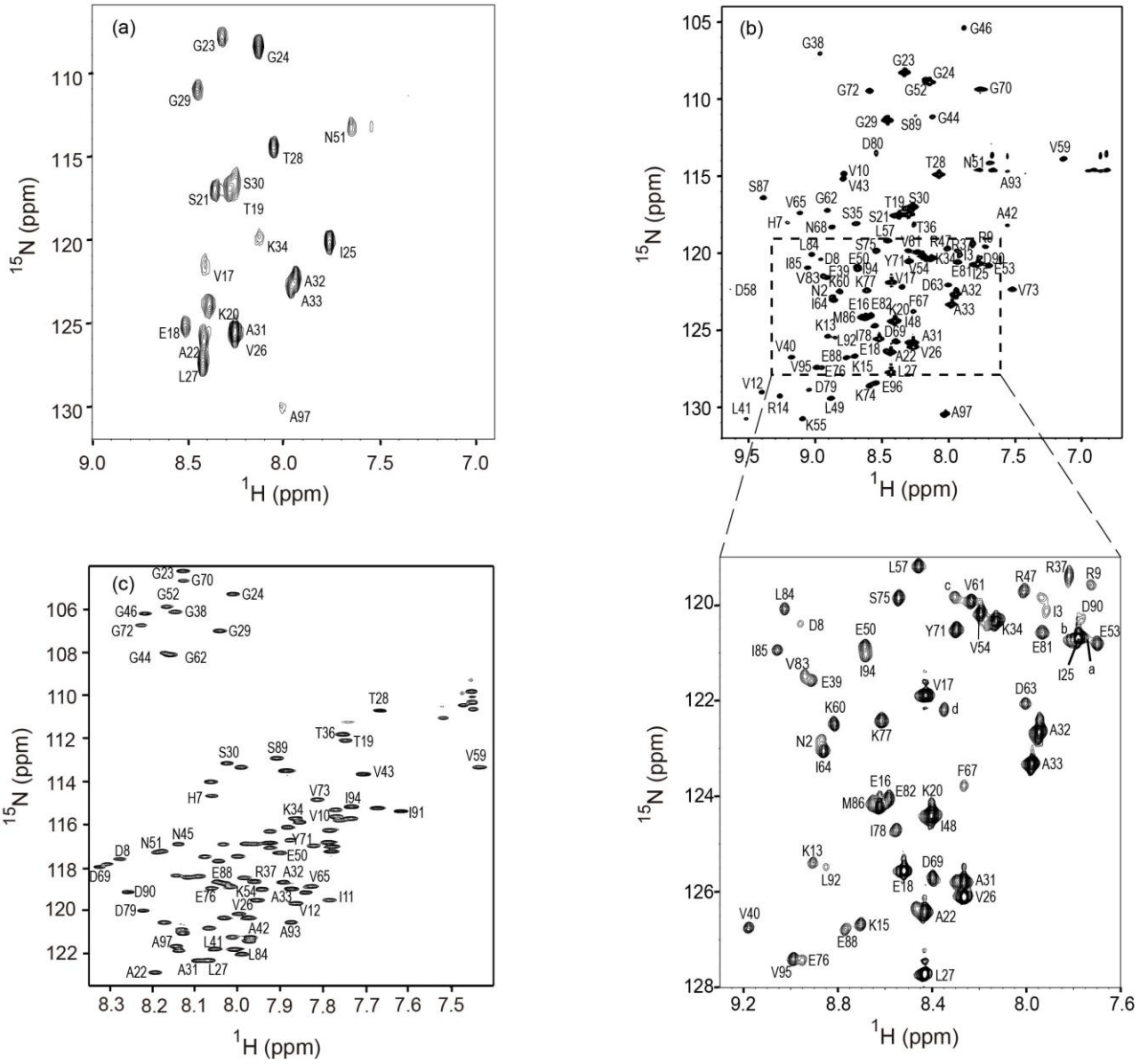

Figure 3-2. 2D NMR spectra of GroES. (a) A ^{1}H 500-MHz [^{15}N, ^{1}H]-HSQC spectrum of uniformly ^{15}N-labeled native GroES in 90% H_2O/10% D_2O at pH 6.5 and 25 °C. (b) A ^{1}H 920-MHz [^{15}N, ^{1}H]-TROSY-HSQC spectrum of {D, ^{15}N}-labeled native GroES in 90% H_2O/10% D_2O at pH 6.5 and 25 °C. The crowded region enclosed by a broken framed rectangle is expanded under the main panel. The cross-peaks labeled by **a**, **b**, **c**, and **d** indicate four unidentified amide protons. (c) A ^{1}H 920-MHz [^{15}N, ^{1}H]-HSQC spectrum of uniformly ^{15}N-labeled unfolded GroES in the DMSO solution (95% DMSO-d_6/5% D_2O, pH* 5.0) at 25 °C.

3.2.2. H/D-exchange kinetics of GroES

Changes in the NMR spectra during H/D-exchange reactions

The H/D-exchange reaction of the protein was started by 10-fold dilution of 3 mM (0.43 mM as the heptamer) ^{15}N-labeled GroES in 25 mM phosphate buffer in H_2O at pH 6.5 into 25 mM phosphate buffer in D_2O at pH* 6.5 at 25.0°C, and the reactions of the amide protons were directly monitored by the $^{1}H–^{15}N$ TROSY HSQC spectra.

Figure 3-3 shows typical spectra observed at different exchange times, 4.6, 27.4, and 161.9 h. Because the first time point, which included a half of the recording time and a time required for adjustment of the NMR spectrometer, was already 4.6 h after starting the H/D-exchange, I could monitor only slowly-exchanging amide protons in the TROSY experiments. Interestingly, however, I observed all the amide-proton signals of residues 17–34 and residues 51–53. Residues 17–34 are in the mobile loop region, and residues 51–53 are located at the top of a roof hairpin loop.[19, 97] These residues were not highly protected, as indicated by the DMSO-QHX as well as direct HSQC H/D-exchange experiments (see below). Because the solution contained 10% H_2O, these protons in the flexible regions exhibited significant signal intensities in spite of the H/D exchange of the amide protons already saturated at the first time point (4.6 h). To distinguish between such fast-exchanging amide protons in flexible regions and very slowly-exchanging amide protons that did not show any significant change in signal intensity during the H/D-exchange measurement, I carried out the same H/D-exchange experiment at a higher pH (pH* 7.5), where the intrinsic chemical exchange rates of the amide protons were increased by ten times.[119, 120] As a result, I identified 27 slowly-exchanging amide protons.

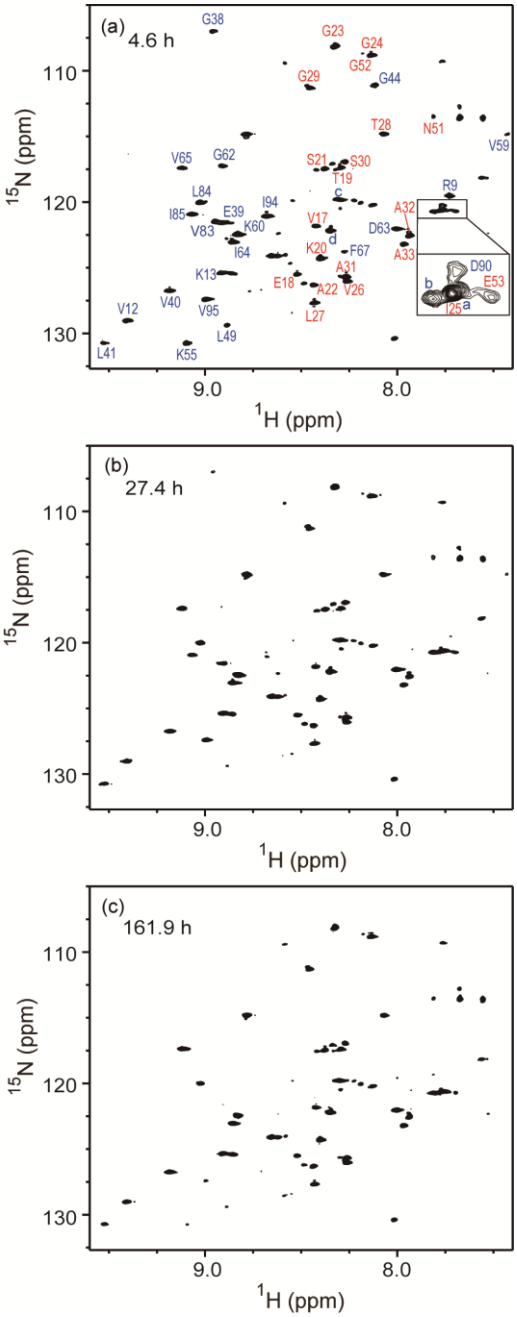

Figure 3-3. [^{15}N, ^{1}H]-TROSY-HSQC spectra of {D, ^{15}N}-labeled GroES in 90% D_2O/10% H_2O at pH* 6.5 and 25 ºC at different H/D-exchange times. The H/D-exchange times are as follows: (a) 4.6 h, (b) 27.4 h, and (c) 161.9 h. The amino-acid residues shown by the one-letter amino acid code plus residue number in blue indicate slowly exchanging amide protons, while those in red indicate fast-exchanging amide protons with significant signal intensities. The four unidentified cross-peaks are labeled as **a**, **b**, **c**, and **d**. All spectra were processed with identical parameters and shown with the same contour levels.

These 27 amide protons consisted of those of Arg9, Gly38, Glu39, Gly44, Leu49, Lys55, Val59, Lys60, Gly62, Ile64, Phe67, Val83, Leu84, Ile85, Asp90, Ile94 and Val95, for which I observed significant exchange-decay kinetics at pH* 6.5, and those of Val12, Lys13, Val40, Leu41, Asp63, Val65 and four as-yet-unidentified residues, for which I observed clear decay kinetics at pH* 7.5. The cross peaks of these residues are labeled by a one-letter amino acid code plus a residue number in blue in Figure 3-3(a); the four unidentified cross peaks are labeled as **a**, **b**, **c**, and **d** in the order of the ^{1}H chemical shift. The chemical shifts of cross peak **a** were coincident with those of the Ile25 cross peak, and the observed cross peak appeared as a composite of two components with very different line widths (inset of Figure 3-3(a)). For the remaining 67 fast-exchanging amide protons, I could not observe the exchange kinetics by TROSY, and the rate constant, k_{ex}, values of the H/D-exchange reactions were estimated to be larger than 0.0002 (=3/(4.6×60×60)) s^{-1}, because more than 95% of the signal intensity change occurred at the first time point (4.6 h).

In the DMSO-QHX experiments, the H/D-exchange reaction of the protein was also started by 10-fold dilution of 3 mM ^{15}N-labeled GroES in H_2O at pH 6.5 into the D_2O buffer solution at pH* 6.5 at 25.0°C. At each pre-determined exchange time, 1.0 mL of the reaction mixture pre-dispensed in a micro-tube was taken, the reaction was quenched in liquid nitrogen, and the frozen mixture was kept in a freezer at −85°C until the medium exchange and the subsequent NMR measurement. For the NMR measurement, the frozen sample was thawed at room temperature, the medium containing 90% D_2O/10% H_2O was exchanged for the DMSO solution by using a spin desalting column,[57] and the ^{1}H–^{15}N HSQC spectrum of the protein was measured. The first time point available in the DMSO-QHX reaction was 20 min, and I measured the exchange reaction until 10 days after starting the H/D-exchange. Moreover, in the DMSO-QHX experiment, I could also obtain the spectrum with no H/D-exchange (Figure 3-2(c)), i.e., at zero time of the H/D-exchange, under the initial H/D-exchange condition by

carrying out the medium exchange of the protein solution in H_2O for the DMSO solution. Figure 3-4 shows $^{1}H–^{15}N$ HSQC spectra of the protein obtained by the DMSO-QHX method with different exchange times, 20 min and 10 days (Figure 3-4(a) and (b)), after starting the H/D-exchange under the H/D-exchange condition (90% D_2O/10% H_2O, pH* 6.5), and with complete exchange by heating the sample under the exchange condition at 70°C for 30 min (Figure 3-4(c)). I obtained the k_{ex} values of 15 amide protons, and the remaining 31 of the 46 assigned amide-protons were too fast to measure by DMSO-QHX, and the k_{ex} values of these fast-exchanging protons were estimated to be larger than 0.0025 (=3/(20×60)) s^{-1}, since more than 95% of the signal intensity change occurred at the first time point (20 min).

I also measured the 18 amide proton cross peaks (residues 17–33, and residue 51 (Asn)), which were observed by the direct $^{1}H–^{15}N$ HSQC spectra of native GroES (Figure 3-2(a)), at different exchange times in 90% D_2O/10% H_2O at pH* 6.5 and 25°C. However, at the first time point (20 min) after starting the H/D-exchange, all these amide protons, except for those of Ser21 and Ile25, were almost fully (approximately more than 90%) exchanged out, indicating that the k_{ex} values of the H/D exchange reactions were larger than 0.002 s^{-1} (= 2.3/(20×60) s^{-1}), since more than 90% of the signal intensity change occurred at 20 min.

3.2.3. Kinetic progress curves of H/D-exchange

I observed H/D-exchange kinetics for 27 slowly-exchanging amide protons, including the four unidentified very slowly-exchanging protons, by TROSY, 15 amide protons by DMSO-QHX, and two amide protons by direct HSQC. Among these amide protons, the exchange reactions of the protons of 7 residues (Gly38, Gly44, Val59, Gly62, Leu84, Asp90, and Ile94) were measured by both TROSY and DMSO-QHX at pH* 6.5.

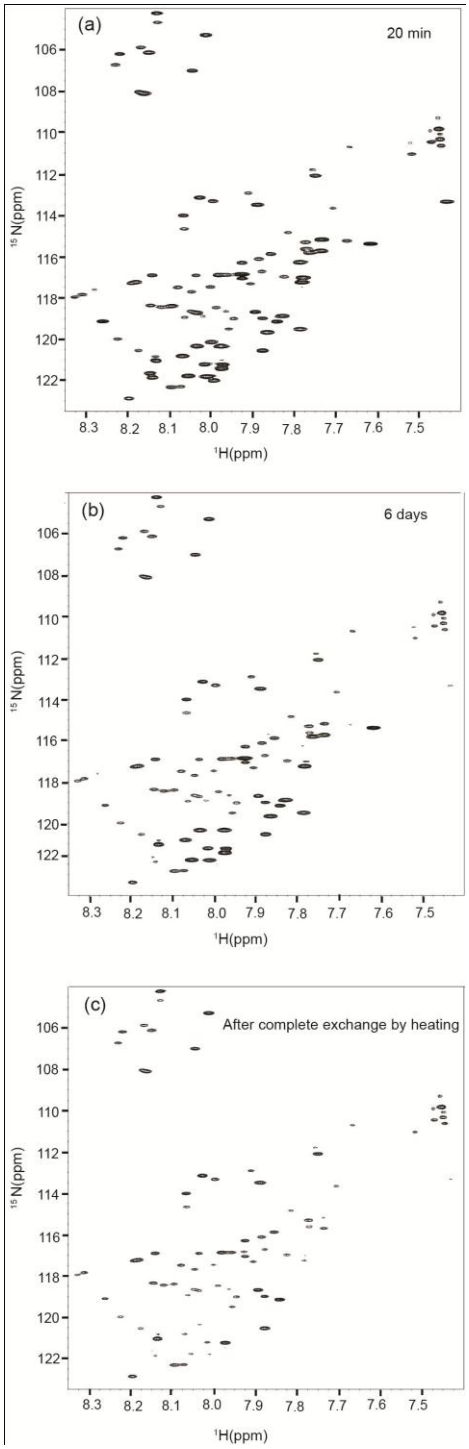

Figure 3-4. (a) [^{15}N, ^{1}H]-HSQC spectra of ^{15}N-labeled unfolded GroES in the DMSO solution at 25 °C with different H/D-exchange times under the H/D-exchange condition (pH* 6.5 and 25 °C), 20 min (a), 6 days (b). The spectrum in (c) is that after complete H/D-exchange by heating at 70 °C for 30 min under the H/D-exchange condition.

All the H/D-exchange kinetics observed were single exponential, and the kinetics measured by TROSY were coincident with those measured by DMSO-QHX except for the kinetics of the Ile94 amide proton, for which the observed H/D-exchange rate constant (k_{ex} = 2.9×10^{-5} s^{-1}) by TROSY was 6 times larger than the rate constant (k_{ex} = 0.45×10^{-5} s^{-1}) measured by DMSO-QHX. The discrepancy in k_{ex} between TROSY and DMSO-QHX remains to be solved, but I employed the value obtained by DMSO-QHX, since my assignment of the Ile94 amide proton in the HSQC spectrum of GroES in the DMSO solution was quite straightforward.

Figure 3-5 shows typical kinetic progress curves of the H/D-exchange reactions of GroES monitored by TROSY and DMSO-QHX. The exchange curve of the Val59 amide proton measured by TROSY showed a single exponential decay with a k_{ex} of 1.7×10^{-5} s^{-1} (Figure 3-5(a)) and this was coincident with the exchange curve measured by DMSO-QHX, which gave a k_{ex} of 1.9×10^{-5} s^{-1} (Figure 3-5(b)). Similarly, the exchange curve of Leu84 measured by TROSY gave a k_{ex} of 0.9×10^{-6} s^{-1} (Figure 3-5(c)), which was coincident with the exchange curve measured by DMSO-QHX, which gave a k_{ex} of 1.3×10^{-6} s^{-1} (Figure 3-5(d)).

Figure 3-6 shows a typical H/D-exchange curve of the fast-exchanging amide proton of Ser21 monitored by direct HSQC. The exchange curve was single exponential, and the k_{ex} value was 0.0014 s^{-1}.

Table 1 summarizes the k_{ex} values of peptide amide protons measured at pH* 6.5 in the present study, and the k_{ex} values of very slowly-exchanging amide protons measured at pH* 7.5 are summarized in Table 2. I obtained the k_{ex} values at pH* 6.5 for 28 out of the 94 expected amide protons either by TROSY, DMSO-QHX, or direct HSQC.

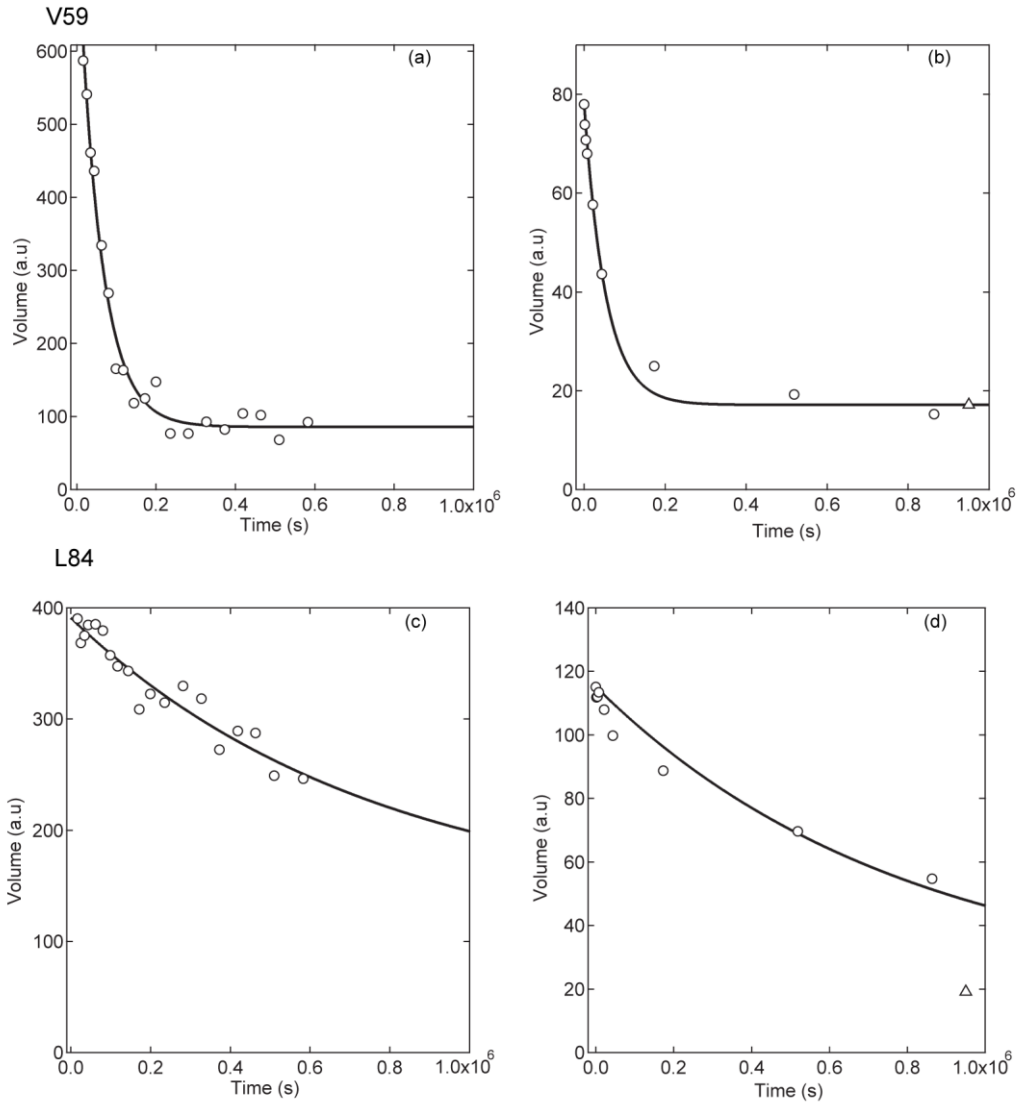

Figure 3-5. Kinetic progress curves of the H/D-exchange reactions of GroES monitored by TROSY [(a) and (c)] and DMSO-QHX [(b) and (d)] (pH* 6.5 and 25°). (a) and (b) indicate the H/D-exchange curves of the Val59 amide proton, and (c) and (d) indicate the H/D-exchange curves of the Leu84 amide proton. Open triangles in (b) and (d) indicate the peak volumes after complete H/D exchange. The thick continuous lines are the theoretical exchange curves fitted to a single-exponential function (Eq. (2-1)) with k_{ex} values of 1.7×10^{-5} s^{-1} (a), 1.9×10^{-5} s^{-1} (b), 0.9×10^{-6} s^{-1} (c), and 1.3×10^{-6} s^{-1} (d).

For very slowly-exchanging amide protons of five residues (Lys13, Val40, Asp63, and the two unidentified residues labeled as **a** and **c** in Figure 3-3(a)), I obtained the k_{ex} values only by TROSY at pH* 7.5; cross peaks **b** and **d** in Figure 3-3(a) were assigned to the amide protons of Ile11 and Ile91 whose exchange rates were also measured at pH* 6.5 by DMSO-QHX (see below). For all the other amide protons, the H/D-exchange rates were too fast to monitor by TROSY, DMSO-QHX or direct HSQC. Therefore, for these 61 fast-exchanging amide protons, the lower limits of k_{ex} are shown in Table 1. The lower limits were: $\log(k_{ex}/s^{-1}) > -3.7$ for the amide protons monitored by TROSY, $\log(k_{ex}/s^{-1}) > -2.6$ for those monitored by DMSO-QHX, and $\log(k_{ex}/s^{-1}) > -2.6$ for those monitored by direct HSQC.

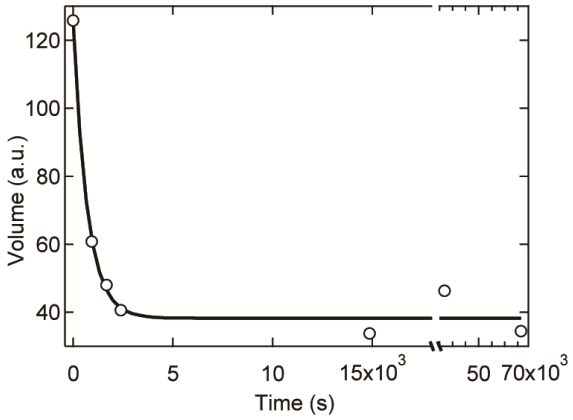

Figure 3-6. A typical kinetic progress curve of the H/D-exchange reaction of the Ser21 amide proton monitored by direct HSQC (pH* 6.5 and 25 °C). The thick continuous line is the theoretical exchange curve fitted to a single-exponential function with a k_{ex} of 0.0014 s^{-1} (Eq. (2-1)).

3.2.4. H/D-exchange progress curves of unidentified amide protons

Figure 3-7 shows H/D-exchange progress curves of the four unidentified and very slowly-exchanging amide protons, which are labeled as **a**, **b**, **c**, and **d** in Fig. 3-3(a), measured by TROSY at pH* 7.5 and 25°C. The k_{ex} values for these protons obtained by fitting to a single-exponential function were 6.2×10^{-7}, 8.5×10^{-7}, 6.3×10^{-7}, and 1.1×10^{-6} s^{-1} for cross peaks **a**, **b**, **c**, and **d**, respectively. For cross peak **a**, which appeared as a composite peak of the very slowly-exchanging amide proton and the fast-exchanging Ile25 proton, I used the difference in the peak volume to extract solely the volume of the very slowly-exchanging component (see the inset of Figure 3-7(a)).

There were five amino-acid residues (Leu6, Ile11, Asn45, Ile66, and Ile91) whose amide-proton cross peaks were not yet identified in the TROSY spectrum,[20] and among these five residues, three residues, Ile11, Asn45, and Ile91, had the cross peaks identified in the HSQC spectrum of unfolded monomeric GroES in the DMSO solution (Figure 3-2(c)). The k_{ex} values for these three residues were thus determined by DMSO-QHX, and they were 2.4×10^{-7}, 0.0018, and 1.7×10^{-7} s^{-1} for Ile11, Asn45, and Ile91, respectively, at pH* 6.5.

The H/D-exchange rate at pH* 7.5 is expected to be ten-fold higher than that at pH* 6.5, and hence the expected k_{ex} values at pH* 7.5 are 2.4×10^{-6}, 0.018, and 1.7×10^{-6} s^{-1} for Ile11, Asn45, and Ile91, respectively. Apparently, the k_{ex} (0.018 s^{-1}) for Asn45 is too fast to measure by TROSY, but those for Ile11 and Ile91 are very close to the measured values of cross peaks **d** and **b**, respectively, at pH* 7.5. I thus assigned cross peaks **d** and **b** to the amide protons of Ile11 and Ile91, respectively. The remaining two cross peaks (**a** and **c**) were thus assigned to the amide protons of Leu6 and Ile66. Because the k_{ex} values of cross peaks **a** and **c** were essentially identical, the k_{ex} values for the two residues were assumed to be 6.2×10^{-7} s^{-1} by taking an

average of the values for cross peaks **a** and **c**. The k_{ex} values thus estimated for Leu6, Ile11, Ile66, and Ile91 are also included in Table 2.

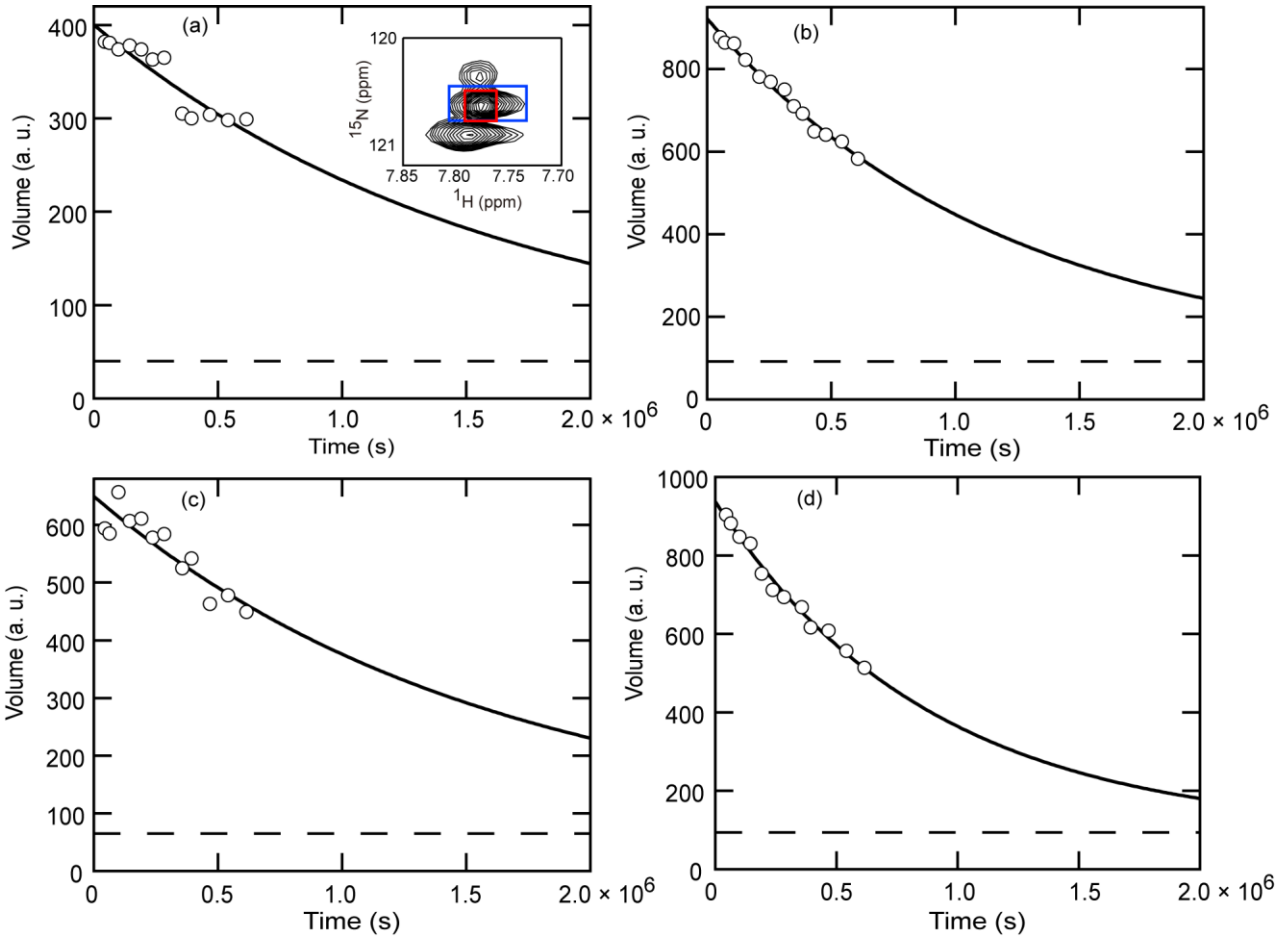

Figure 3-7. The H/D-exchange progress curves of four unidentified amide protons, which are labeled **a**, **b**, **c**, and **d** in Figure 3-3(a), at pH* 7.5 and 25°C. For cross-peak a, which appeared as a composite peak of the very slowly exchanging amide proton and the fast-exchanging Il25 proton, we used the difference in the peak volume to extract solely the volume of the very slowly exchanging component by subtracting the volume enclosed by a red rectangle from the volume enclosed by a blue rectangle (inset of (a)). The broken line in each panel is the peak volume at infinite time. The thick continuous lines are the theoretical exchange curves fitted to a single-exponential function (Eq. (2-1)) with k_{ex} values of 6.2×10^{-7} s^{-1} (a), 8.5×10^{-7} s^{-1} (b), 6.3×10^{-7} s^{-1} (c), and 1.1×10^{-6} s^{-1} (d).

3.2.5. Protection profile

The protection factor, P_f, of each amide proton of the protein is given by a ratio of the rate constant, k_{int}, for the intrinsic chemical H/D-exchange reaction in the freely exposed state of the amide group and the k_{ex} measured by the H/D-exchange experiments (Equation (1-9)). The k_{int} values for the individual amide protons of GroES under the present conditions (pH* 6.5 and 7.5 at 25°C) were evaluated from the amino-acid sequence of GroES by the methods of Bai *et al.*[43] and Connelly *et al.*[44] The P_f values of the individual amide protons of GroES are included in Tables 1 and 2, and Figure 3-8 shows a protection profile that represents log P_f as a function of the residue number. I obtained the P_f values at pH* 6.5 for 28 amide protons (gray bars in Figure 3-8), and the upper limits of P_f at pH* 6.5 for 61 amide protons (sticks and plus marks in Figure 3-8). For the five amide protons of Leu6, Lys 13, Val40, Asp63, and Ile66, I could estimate the P_f values only from the exchange data at pH* 7.5 (blue bars in Figure 3-8), because their exchange reactions were too slow at pH* 6.5.

To investigate the relationships between the protection profile in Figure 3-8 and the secondary structure of GroES, I analyzed the X-ray crystallographic structure of the GroES portion of the GroEL/GroES/ADP complex (PDB code: 1AON)[12] by the method of Kabsch and Sander;[118] the PDB coordinates for standalone heptameric GroES are not yet published although its X-ray structure was reported.[19] The secondary structure of GroES consists of seven β-strands, several reverse turns, a 3_{10}-helix, and two loop regions (Figure 3-1). The seven β-strands are labeled as A, B, C, D, E, F, and G in the order from the N-terminal to the C-terminal side, and they are shown at the top of Figure 3-8. The highly protected amino-acid residues with P_f values larger than 10^5 are mainly located in three β-strands (strands B, C, and D) that form the hydrophobic core of GroES, while the residues in the mobile loop (residues 17–34) are not highly protected (Figure 3-8).

3.3. Discussion

I studied the H/D-exchange kinetics of individual amide protons of native heptameric GroES at pH* 6.5 and 7.5 at 25°C. The use of the TROSY and DMSO-QHX techniques has made it possible to investigate the H/D-exchange behaviors of the individual identified amide protons of the protein supermolecular complex GroES, for which the conventional 2D NMR techniques could not give us much information.

By using these techniques together with the direct HSQC experiments, I could quantitatively evaluate the k_{ex} values for 33 out of the 94 peptide amide protons and their P_f values, and for the remaining 61 residues, I obtained the lower and the upper limits of the k_{ex} and P_f values, respectively (Tables 1 and 2) (Figure 3-8). The P_f values of the most highly protected amide protons were on the order of 10^6–10^7, and they were comparable in magnitude to those observed in typical small globular proteins, which have a molecular weight of 10,000–20,000.[119, 121]

However, the number of highly protected amide protons with P_f values larger than 10^6 was only ten from Figure 3-8, significantly smaller than the numbers reported for the small globular proteins, e.g., more than 24 for barnase,[122] a 110-residue protein, and 36 for staphylococcal nuclease,[120] a 149-residue protein. Apparently, significant portions of GroES with P_f values less than 10^4 are not highly protected, although the most highly protected protons are protected to the same degree as observed in the small globular proteins. The 3D structure of GroES, the monomeric unit and the heptameric complex, are shown in Figure 3-1(a) and (b), respectively. The structure is presented in different colors according to the P_f values (red for $P_f < 10^4$, yellow for $10^4 \leq P_f < 10^5$, cyan for $10^5 \leq P_f < 10^6$, and blue for $10^6 \leq P_f$).

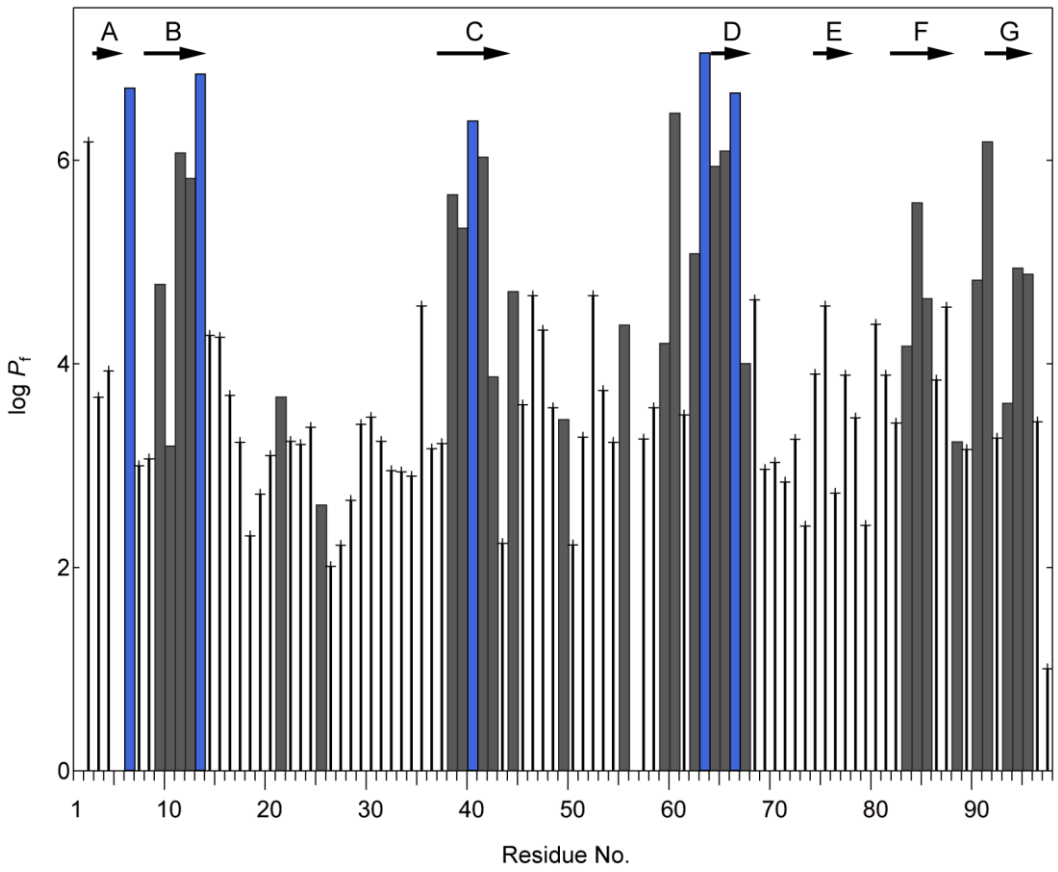

Figure 3-8. The H/D-exchange protection profile represented by log P_f as a function of the residue number. The gray and blue bars indicate the P_f values at pH* 6.5 (28 amide protons) and pH* 7.5 (5 amide protons), respectively. The sticks and plus marks indicate the upper limits of P_f at pH* 6.5 (61 amide protons)

The structure of the GroES subunit consists of an irregular β-barrel formed by strands B, C, D, E and F, two loop regions, several reverse turns, a short 3_{10}-helix (residues 87–91), and the N- and C-terminal β-strands (strands A and G) that are located at the subunit-subunit interface (Figure 3-1).[12, 19, 101, 108] The highly protected amide protons with P_f values larger than 10^5 are located in four regions of the GroES molecule, i.e., the major hydrophobic core formed mainly by three β-strands, B, C and D, a stable type-II β-turn formed by residues 60–63, the 3_{10}-helix of residues 87–91, and the subunit-subunit interface formed by Leu6 of one subunit and Ile91 of the

preceding subunit. Strand A, strand E, and the two loop regions are not highly protected, and the P_f values for most residues are less than 10^4 (Figure 3-8).

In the following, I am going to discuss further details of the H/D-exchange behaviors of GroES. In addition, I will also discuss the effective thermodynamic stability of GroES, evaluated from the P_f values of the most highly protected amide protons (Equation (1-12)),[119, 121, 123] and the relationship of the thermodynamic stability with the equilibrium unfolding parameters of GroES previously reported.[109-113, 124]

3.3.1. The H/D-exchange behaviors

The most prevalent mechanism of the H/D-exchange protection is hydrogen bonding, and the hydrogen bond is thus broken before a protected amide proton is exchanged with a solvent deuteron.[120, 125] In fact, all the highly protected amide protons ($P_f > 10^5$) except for those of Lys60 and Ile64 are hydrogen-bonded to a peptide carbonyl oxygen of the same chain or an adjacent chain.[12, 19, 101, 108] The amide proton of Lys60 is hydrogen-bonded to the side-chain O^{δ} atom of Asp63. For the Ile64 amide proton, however, there is no possible acceptor group in the X-ray structural coordinates of GroES currently published in the protein data bank (PDB codes: 1AON, 1PCQ, 1PF9, 1SVT and 1SX4).[12, 101, 108] A possible protection mechanism for the Ile64 amide proton is thus the hydrogen bonding to a water molecule that is strongly hydrated and integrated into the native protein structure,[120,125] although crystallographically determined water molecules are not observed around the GroES portion of the currently published PDB coordinates.†

Footnote † In the PDB coordinate of the refined X-ray structure of stand-alone GroES (J. F. Hunt, personal communications), we find water molecules that are hydrogen-bonded to the Ile64 amide groups

The major hydrophobic core

The major hydrophobic core of GroES is organized by strands B, C and D; ten residues in these β-strands, i.e., Ile11, Val12 and Lys13 in strand B, Gly38, Glu39, Val40 and Leu41 in strand C, and Ile64, Val65 and Ile66 in strand D have a P_f value larger than 10^5. In addition to these residues, Leu84 of strand F, and Ile91 of strand G are highly protected, with P_f values larger than 10^5, and their side chains are directly in contact with the major hydrophobic core formed by strands B, C, and D, further stabilizing the hydrophobic core of GroES. The side chain of Ile91 also makes hydrophobic contacts with the side chain of Leu6 of the next adjacent side chain, providing continuous hydrophobic interactions through the seven subunits of the GroES heptamer.[12, 19, 101, 108]

Turns and a 3_{10}-helix

There are five turn conformations and one 3_{10}-helix in the monomeric unit of GroES, i.e., five reverse turns of residues 6–9, 49–52, 60–63, 70–73 and 78–81, and a 3_{10}-helix of residues 87–91;[12, 19, 101, 108] I ignored residues 17–34 of the mobile loop which is natively unfolded in free heptameric GroES. Among the residues of these turns and helix, Lys60, Gly62 and Asp63 in residues 60–63 (type-II β-turn) and Asp90 in residues 87–91 (3_{10}-helix) are highly protected, with P_f values larger than 10^5 (Tables 1 and 2, and Figure 3-8). Residues 60–63 are between the D strand and the roof hairpin (residues 44–58), and the Asp63 amide proton is hydrogen-bonded to the peptide carbonyl oxygen of Lys60. The amide proton of Lys60 is hydrogen-bonded to the side chain O^{δ} of Asp63, and the Gly62 amide proton is hydrogen-bonded to the peptide carbonyl oxygen of Val40 in the C strand, producing a β-bulge structure at the N-terminal end of strand D. Residues 87–91 form a two-turn 3_{10}-helix between strands F and G, and the Asp90 amide proton is hydrogen-bonded to the carbonyl oxygen of Ser87.

The subunit-subunit interface

The amide protons of Ile91 and Leu6 are very highly protected, with P_f values larger than 10^6 (Tables 1 and 2, and Figure 3-8), and the structure at the subunit-subunit interface is shown in Figure 3-9. The Ile91 amide proton is hydrogen-bonded to the carbonyl oxygen of Glu88, forming a part of the 3_{10}-helix of residues 87–91. The side chain of Ile91 makes hydrophobic contacts with the Leu6 side chain of the next adjacent chain. The Leu6 amide proton is hydrogen-bonded to the Leu92 carbonyl oxygen of the preceding chain of GroES, and this hydrogen bonding and the hydrophobic contacts between the N- and C-terminal regions of the adjacent chains are the interactions that stabilize the subunit-subunit interface.[12, 19, 101, 108] The importance of the C-terminal residues (Ile91 and Leu92) for the subunit-subunit interactions was also indicated by a C-terminal truncation experiment, in which the removal of the seven C-terminal residues prevented the heptamer formation of GroES.[126] Sakane *et al*.[112] also reported that the introduction of mutations that decreased hydrophobic contacts between the N- and C-terminal regions decreased the stability of the GroES heptamer.

Loop regions

There are two loop regions in the monomeric unit of GroES, i.e., the mobile loop of residues 17–34 and the roof hairpin loop of residues 44–58. All the amide protons in the mobile loop region are unprotected, and their P_f values are less than 10^4 (Table I). The mobile loop region is natively unfolded, and its amide proton signals are observed by 2D NMR with the chemical shift values expected for a random chain (Figure 3-2(a)).[97]

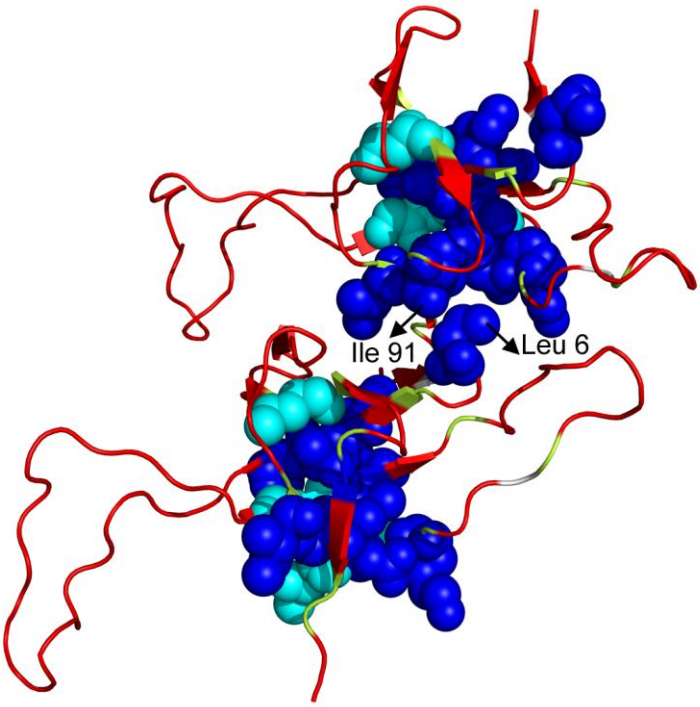

Figure 3-9. The structure at the subunit–subunit interface of GroES (PDB code: 1AON). Two adjacent subunits of the GroES heptamer are shown, and the residues that have a P_f value larger than 10^5 are shown by a space-filling model. Leu6 and Ile91 are labeled. The structure is classified by different colors according to the P_f values as in Figure 3-1. The figure was prepared using PyMOL (DeLano Scientific).

The results are consistent with the reported crystal structure of GroES, in which the mobile loop segment was disordered in the crystal structure in six out of the seven subunits.[19] The natively unfolded nature of the mobile loop is crucial for recognition by the chaperonin GroEL and the chaperonin cycling of the GroEL/GroES complex mediated by ATP hydrolysis.[98-100]

The roof hairpin of residues 44–58 is also not highly protected, with P_f values less than 10^5, and the amide proton of Asn51 that is located at the top of the roof hairpin was observed by the direct HSQC spectrum (Figure 3-2(a)), indicating the flexible nature of the reverse turn (residues

49–52). The amide protons of two residues, Gly44 and Lys55, are, however, significantly protected, with P_f values of 4.9×10^4 and 2.4×10^4, respectively, indicating that the base and middle portions of the hairpin strands are not fully flexible. The amide protons of Gly44 and Ly55 are hydrogen-bonded to the carbonyl oxygen of Arg9 and Arg47, respectively.[12, 19, 101, 108]

3.3.2. Effective thermodynamic stability of GroES

Among the 10 highly protected residues with P_f values larger than 10^6, four residues, i.e., Leu6, Lys13, Asp63 and Ile66, are the most highly protected, with an average P_f of 6.7×10^6 (Tables 1 and 2). These most highly protected amide protons are exchanged out through the global unfolding of GroES, and hence the P_f value is related to the effective thermodynamic stability (ΔG_{eff}) of global unfolding as indicated by Equation (1-12).[119, 121, 123] The ΔG_{eff} thus obtained is 9.3 kcal/mol. However, the ΔG_{eff} of an oligomeric protein depends on the protein concentration, and for a heptameric protein, GroES, the dependence of ΔG_{eff} on the molar concentration, C, of the GroES monomer unit is given by[112, 127]

$$\Delta G_{eff} = \frac{\Delta G^\circ}{7} + \frac{RT}{7}\ln(7\cdot C^6) \qquad (3\text{-}1)$$

where ΔG° is the standard free-energy change that is independent of the protein concentration, and $\Delta G^\circ/7$ is the ΔG° per monomer unit. The molar concentration C of GroES in *E. coli* cells is reported to be about 35 μM in monomer units,[115-117] and under a stress condition, the concentration may be ten times higher (~350 μM).[115] The GroES concentration in the present study (300 μM) was within this range, and the ΔG_{eff} shown above (9.3 kcal/mol) is thus physiologically relevant. The ΔG_{eff} of 9.3 kcal/mol at 300 μM gives a ΔG° of 92.8 kcal/mol at 298.15 K, and at 35 μM, the ΔG_{eff} is thus estimated at 8.2 kcal/mol from Equation (3-1) using this ΔG°. Although Equation (3-1) is based on a simple two-state model of unfolding (see

below),[127] the direct observation of the P_f values by the H/D-exchange and the above estimates of ΔG_{eff} clearly indicate that the effective thermodynamic stability of GroES under physiological conditions is on the order of 8–10 kcal/mol. The effective thermodynamic stability of GroES is thus well designed so as to be comparable to the stability of typical small globular proteins, which is usually between 5 and 15 kcal/mol,[128] at physiological concentrations of GroES. An advantage of the H/D-exchange technique is that we can directly evaluate the effective thermodynamic stability of proteins and protein assemblies by Equation (1-12) without any presumed models and extrapolations.

3.3.3. Global unfolding of GroES

The equilibrium unfolding transitions of GroES induced by denaturants (GdmCl and urea) and by increasing temperature have been studied by a variety of techniques, including sedimentation equilibrium and velocity experiments,[109, 124] intrinsic and extrinsic fluorescence spectroscopy,[109,111,113] circular dichroism spectroscopy,[110,113] differential scanning calorimetry,[110] size-exclusion chromatography,[111,112] and small-angle X-ray scattering.[114] The ΔG_{eff} can also be estimated from the equilibrium unfolding experiments, but unlike in the case of the H/D-exchange, we need to extrapolate the free-energy change of unfolding obtained under unfolding conditions to the native physiological condition on the basis of a certain presumed model (two-state unfolding, three-state unfolding or other) used for analysis of the experimental data. For a simple two-state unfolding of a monomeric protein, the linear-free-energy relationship with respect to the denaturant concentration has been well established,[129] and we can easily extrapolate the free-energy change to the native condition. However, for an oligomeric protein, the free-energy relationship is not that simple; the free energy also depends on the protein concentration (Equation (3-1)). Here, I thus compare the present results of the most

stably protected amide protons (P_f = 6.7×10^6, and ΔG_{eff} = 9.3 kcal/mol) and the known results of the equilibrium unfolding of GroES.[109-113, 124]

Two-state model

The simplest model of the equilibrium unfolding of free heptameric GroES involves a two-state unfolding equilibrium between the heptameric native state, N_7, and the monomeric unfolded state, U, and the previous studies on the GroES unfolding often employed the two-state unfolding model.[109, 110, 113] The unfolding transition is thus represented by

$$N_7 \underset{}{\overset{K_U}{\rightleftarrows}} 7U \qquad (3\text{-}2)$$

where K_U is the equilibrium constant of unfolding, and K_U and the free-energy change, ΔG_U, of unfolding are given by

$$K_U = \frac{[U]^7}{[N_7]} \qquad (3\text{–}3)$$

$$\Delta G_U = -(RT \ln K_U)/7 \qquad (3\text{–}4)$$

where [N_7] and [U] are the molar concentrations of N_7 and U, respectively, and ΔG_U is the free-energy change per mol of the GroES monomer. If we assume that the H/D-exchange rate in the U state is identical to the intrinsic chemical exchange rate k_{int} in the freely exposed state, the observed exchange rate constant k_{ex} based on the EX2 mechanism is given by[123]

$$k_{ex} = \frac{[U]}{7[N_7]+[U]} k_{int} \approx \frac{[U]}{7[N_7]} k_{int} = \frac{(K_U[N_7])^{1/7}}{7[N_7]} k_{int} = \frac{e^{-\Delta G_U/RT}[N_7]^{1/7}}{7[N_7]} k_{int} \quad (3\text{-}5)$$

where [U] « 7[N_7], and the protection factor P_f is thus given by

$$P_f = \frac{7[N_7]}{(K_U[N_7])^{1/7}} = \frac{7[N_7]}{e^{-\Delta G_U/RT}[N_7]^{1/7}} . \qquad (3\text{-}6)$$

This equation is equivalent to Equation (3-1), but here we calculate P_f values from the K_U or ΔG_U values previously reported, and compare the calculated values with the P_f value (6.7×10^6) directly obtained by the H/D-exchange.

Boudker *et al.*[110] analyzed the thermal unfolding and the unfolding of GroES by a denaturant, urea, by assuming the two-state model, and reported the ΔG_U values between 8 and 10.2 kcal/mol. Luke and Wittung-Stafshde[113] also carried out similar analyses of the equilibrium unfolding transitions of heptameric co-chaperonin proteins 10 from different species, including *E. coli* GroES, and reported the ΔG_U values between 7.9 and 8.6 kcal/mol for GroES. By assigning these values of ΔG_U and the molar concentration of N_7 ($[N_7] = 4.3\times10^{-5}$ M) in the present study to Equation (3-6), we obtain a P_f value of $(0.99–38)\times10^3$ (i.e., ΔG_{eff} = 4.1–6.2 kcal/mol). Apparently, the P_f value thus obtained is not consistent with the experimental P_f value (6.7×10^6) for the most highly protected amide protons, indicating that the simple two-state model of the GroES unfolding does not explain the H/D-exchange behavior of GroES. Zondlo *et al.*[124] carried out sedimentation equilibrium experiments for the GroES heptamer, and obtained a dissociation constant of 1×10^{-38} M^6. If we assume the simple two-state unfolding model and assign this value to K_U in Equation (3-6), we obtain a P_f of 3.4×10^2 (ΔG_{eff} = 3.5 kcal/mol), which is again much smaller than the experimental P_f value, indicating that the simple two-state model is not consistent with the present H/D-exchange results.

Three-state model

The Kawata group studied the GdmCl-induced unfolding of GroES by 1-anilino-8-naphtalene sulfonate binding, intrinsic fluorescence spectroscopy, size-exclusion HPLC analysis and

solution X-ray scattering,[111, 112, 114] and they found the presence of a monomeric folded intermediate of GroES during the unfolding transition. The unfolding of GroES thus occurs in at least two steps, (1) the dissociation of heptameric GroES into folded monomers, and (2) the unfolding of the folded monomer, as

$$N_7 \xrightleftharpoons{K_d} 7M \tag{3-7}$$

$$M \xrightleftharpoons{K_u} U \tag{3-8}$$

where M represents the folded monomer, and K_d and K_u are the dissociation constant of N_7 into seven monomers and the unfolding equilibrium constant between M and U, respectively. If we assume that the H/D-exchange reactions of the most stable protons occur only in the U state and that the exchange rate in the U state is identical to the k_{int}, the observed exchange rate constant k_{ex} is given by

$$k_{ex} \approx \frac{[U]}{7[N_7]} k_{int} = \frac{K_u (K_d [N_7])^{1/7}}{7[N_7]} k_{int} = \frac{e^{-\Delta G_u / RT} e^{-\Delta G_d / RT} [N_7]^{1/7}}{7[N_7]} k_{int} \tag{3-9}$$

where the concentrations of M and U are negligible compared with $7[N_7]$, and the protection factor P_f is thus given by

$$P_f = \frac{7[N_7]}{K_u (K_d [N_7])^{1/7}} = \frac{7[N_7]}{e^{-\Delta G_u / RT} e^{-\Delta G_d / RT} [N_7]^{1/7}} \tag{3-10}$$

According to Sakane *et al*.,[112] $K_d = 1.7\times10^{-37}$ M^6, and $K_u = 2.1\times10^{-2}$. By assigning these values to Equation (3-10), we obtain a P_f value of 7.7×10^3 (ΔG_{eff} = 5.3 kcal/mol), which is again a few orders of magnitude smaller than the P_f value in the present study.

3.3.4. A possible molecular mechanism of the GroES unfolding

If the two-state and the three-state models of the GroES unfolding are not consistent with the H/D-exchange behavior of GroES, what kinds of molecular mechanisms of the GroES unfolding are possible? Although the results of the H/D-exchange experiments do not directly reveal the unfolding mechanism of GroES, the P_f values calculated from the previous two-state and three-state unfolding data were always a few orders of magnitude smaller than the P_f value (6.7×10^6) for the most highly protected amide protons in the present study, strongly suggesting that there are additional intermediates that were not taken into account in the previous models of GroES unfolding. I thus here hypothesize that such intermediates may be partially dissociated oligomeric species (hexamer, pentamer, tetramer, trimer and dimer) of GroES, which were not considered in the previous models that assumed simultaneous dissociation from a heptamer to seven monomers (Equations (3-2) and (3-7)).

In support of this hypothesis, Sakane *et al.*[130] and Ikeda-Kobayashi *et al.*[131] recently reported that mechanical unfolding of covalently linked GroES showed a distinctive sawtooth pattern that is typical for multimodular proteins, indicating the presence of such intermediates in which a subset of the subunits were detached and disrupted. The presence of such intermediates can reasonably explain the discrepancy between the previously reported equilibrium unfolding parameters and the P_f value in the present study, because the presence of the additional intermediates makes the unfolding transition less cooperative, leading to a smaller apparent unfolding free energy when analyzed the apparent unfolding transition by the simple two-state or three-state model. Nevertheless, further studies will be needed to elucidate the presence of such partially dissociated intermediates in wild-type GroES with no covalent links.

Another possibility that should also be considered for interpreting the discrepancy between the P_f values calculated from the previous unfolding data and those directly measured in the present H/D-exchange experiments might be that the unfolded monomer retained some residual structure in certain regions, resulting in "hyper-protection" and P_f values in excess of the value calculated from the equilibrium unfolding data. In fact, the presence of residual structure in the unfolded state was reported in an H/D-exchange study of cyt *c*.[46] However, the protection factor in the unfolded state was reported to be on the order of 30,[46] much smaller than the protection factor, 2×10^2–2×10^4, expected from the above discrepancy between the P_f values. Furthermore, the residual structure in the unfolded state of cyt *c* arose from a cyclic structure stabilized by the heme thoiether bridges and the His18 to heme coordination.[46] In GroES, there is no such a covalent or coordination bond. A survey of the H/D-exchange literature found many proteins for which the slowest-exchanging amide protons when processed through Equation (1-12) yield ΔG_{eff} values that closely match the unfolding free-energy values obtained by standard protein unfolding experiments,[119, 121, 123] further strengthening the above conclusion that there are additional intermediates that were not taken into account in the previous models of GroES unfolding.

3.4. Materials and methods

3.4.1. Materials

^{15}N-labeled and {^{13}C, ^{15}N}-double-labeled GroES proteins were expressed in *E. coli* host cells BL21(DE3) at 37°C in M9 minimal medium using the expression plasmid pETESwild, which was a gift of Professor Y. Kawata (Tottori University,Japan).[114] The expression was induced with IPTG when the optical density of the culture medium was 0.6, and the cells were grown for

4–5 h after the induction. Perdeuterated and ^{15}N-labeled GroES ({D, ^{15}N}-GroES) was expressed in the *E. coli* cells grown in M9 minimal medium prepared in D_2O. The cells expressing the protein were collected by centrifugation and lysed by sonication in 50 mM Tris-HCl buffer (pH 7.5) that contained 2 mM EDTA, 0.1 mg/ml DNase, 4 mM $MgCl_2$ and components in a tablet of complete protease inhibitor cocktail (Roche). The lysate was centrifuged at 17,000 rpm for 1 h at 4°C, and the supernatant was heated at 80°C for 20 min. After the heat treatment, the mixture was quickly cooled on ice for 30 min. To remove heat-denatured proteins, the heated mixture was centrifuged at 17,000 rpm for 40 min at 4°C. The supernatant was precipitated with 55% saturation of ammonium sulfate for overnight at 4°C. The precipitate was collected by centrifugation at 17,000 rpm for 60 min at 4°C, and dissolved in Buffer A (50 mM Tris, pH 7.5 and 2 mM EDTA). The soluble fraction of cell lysate was applied to a Sephacryl S-300 HR column equilibrated with Buffer A. The fractions containing GroES were pooled, and further purified on a Q Sepharose FF column (250 mL) equilibrated with Buffer A with a linear gradient of NaCl from 0.20 to 0.50 M.[84,114] The purified GroES was stored at −20°C in Buffer A, which contained 15% (v/v) glycerol, to avoid degradation. The concentration of GroES was measured by UV absorption at 280 nm using an extinction coefficient, $E_{1cm}^{0.1\%} = 0.143$, for GroES.[84]

The Zeba™ Spin Desalting Columns used in the DMSO-QHX experiments[57] were purchased from Thermo Scientific (Rockford, IL, USA). DMSO-d_6 (99.9% D) and D_2O (99.9% D) were from Cambridge Isotope Laboratories (Andover, MA, USA). All other chemicals were of guaranteed reagent grade.

3.4.2. H/D-exchange measurements

All the H/D-exchange experiments were carried out in Buffer B (25 mM phosphate and 20 mM KCl) at 25°C, and the molar concentration of GroES (heptamer) was 43 μM. The H/D-

exchange reaction was started by the ten-fold dilution of 430 μM GroES in the H_2O buffer into the D_2O buffer; the solution thus contained 10% H_2O and 90% D_2O. The pH* value was 6.5, and in the TROSY experiments, the measurements were also carried out at pH* 7.5. All NMR spectra were processed and analyzed by NMRPipe[75] and NMRView.[76]

TROSY experiments

{D, ^{15}N}-GroES was used in the TROSY experiments, and 2D ^{1}H–^{15}N TROSY spectra were recorded on a JEOL ECA-920-MHz NMR spectrometer every 2.5 h for one week during the H/D exchange at 25°C. I acquired 32 transients for each of 256 t_1 points, and the sweep widths in t_1 and t_2 were 2799 and 14988 Hz, respectively. The data acquisition for the first time point was started at approximately 3.3 h after the H/D-exchange was started, and hence, the first time point was set at 4.6 h (= 3.3+2.5/2 h)

Direct HSQC experiments

2D ^{1}H–^{15}N fast HSQC NMR spectra were recorded on a Bruker AVANCE 500 MHz NMR spectrometer every 12 min for 20 h during the H/D-exchange at 25°C. The ^{1}H flip angle was optimized at 75° for the fast HSQC measurement. The data acquisition for the first time point was started at 14 min after the H/D-exchange was started, and the first time point was set at 20 min (= 14+12/2 min).

DMSO-QHX experiments

For the H/D-exchange experiments, a frozen stock GroES solution kept at −20°C was thawed, and the buffer was exchanged for Buffer B (25 mM phosphate and 20 mM KCl at pH 6.5) using a PD-10 desalting column (GE Healthcare). After adjusting the GroES concentration to 430 μM in heptamers, the H/D-exchange reaction was started by 10-fold dilution of the GroES solution into Buffer B prepared in D_2O (pH* 6.5), giving the final GroES concentration of 43 μM (300 μM in monomer units). Immediately after the dilution, 1.0 mL of the reaction mixture was dispensed into each of 10–20 microtubes with a screw cap sealed by an O-ring to prevent water contamination, and the solutions in the tubes were incubated at 25.0°C for H/D-exchange. At each pre-determined exchange time between 20 min and 10 days, the reaction mixture in a tube was taken, and the reaction was quenched in liquid nitrogen. The frozen mixtures were kept in a freezer at −85°C until the medium exchange and the subsequent NMR measurement. For the NMR measurement, the frozen sample was first thawed at room temperature, and the medium containing Buffer B in 90%D_2O/10%H_2O was exchanged for the DMSO solution (95% DMSO-d_6/5% D_2O and pH* 5.0) by using a spin desalting column (Zeba^{TM} Spin Desalting Column 89891, 5 mL; Thermo Scientific) as described by Chandak *et al*.[57] The ^{1}H–^{15}N HSQC spectrum of the protein in the DMSO solution was measured on a JEOL ECA-920-MHz NMR spectrometer at 25°C. I acquired 16 transients for each of 256 t_1 points, and the sweep widths in t_1 and t_2 were 2,426 and 13,827 Hz, respectively. The extent of H/D- exchange at each time point was determined by the volume of each cross-peak in the HSQC spectrum.

To achieve the backbone resonance assignment of GroES in the DMSO solution, 3D CBCACONH and HNCACB experiments were performed on a JEOL ECA-920 MHz spectrophotometer at 25°C, and the ^{1}H, ^{13}C and ^{15}N chemical shifts have been deposited in the BioMagResBank (http://www.bmrb.wisc.edu) under accession number BMRB-18949.

3.4.3. Data analysis

The observed kinetic exchange curves were calculated as described in Chapter 2 (Equation (2-1)). For the H/D-exchange reactions directly measured in the NMR probe (TROSY and direct HSQC), the Y_∞ value in Equation (2-1) was expected to be 10% of the initial peak volume because the protein solution for the H/D-exchange, being identical to the solution for the NMR measurement, contained 10% H_2O. For the DMSO-QHX experiments, however, the Y_∞ value was unpredictable because the H/D exchange was not completely quenched in the DMSO solution, so that an additional exchange occurred in the DMSO solution during the NMR measurement (more detailed descriptions are given in Chapter 2, page 48). In the DMSO-QHX experiments, I thus prepared a protein solution after complete exchange in Buffer B (90% D_2O/10% H_2O) by keeping the solution at 70°C for 30 min, and measured the NMR spectra of the completely-exchanged protein in the DMSO solution to obtain the Y_∞.

Table 1. H/D-exchange parameters of GroES at pH* 6.5 and 25 °C

Residue	k_{int} (s^{-1})	log(k_{ex}/s^{-1})	log P_f	Methods[a]	Residue	k_{int} (s^{-1})	log(k_{ex}/s^{-1})	log Pf	Methods
N2	2.76×10^{2}	> −3.74[b]	< 6.18[b]	T	A32	2.16	> −2.62	< 2.95	H
I3	0.842	> −3.74	< 3.67	T	A33	2.16	> −2.60	< 2.94	D
R4	1.53	> −3.74	< 3.93	T	K34	1.97	> −2.60	< 2.90	D
P5	—	—	—	—	S35	6.68	> −3.74	< 4.57	T
L6	0.328	n.a.	n.a.		T36	3.67	> −2.60	< 3.17	D
H7	2.50	> −2.60	< 3.00	D	R37	4.12	> −2.60	< 3.22	D
D8	2.92	> −2.60	< 3.07	D	G38	6.68	−4.84	5.67	T, D
R9	1.73	−4.55	4.79	T	E39	0.996	−5.35	5.34	T
V10	0.717	−3.34	3.20	D	V40	0.308	< −6.77	> 6.25	T
I11	0.293	−6.62	6.08	D	L41	0.413	−6.42	6.04	D
V12	0.255	−6.43	5.83	D	A42	1.33	−3.75	3.88	D
K13	1.43	< −6.77[c]	> 6.92[c]	T	V43	0.432	> −2.60	< 2.24	D
R14	3.43	> −3.74	< 4.28	T	G44	2.92	−4.25	4.72	T, D
K15	3.27	> −3.74	< 4.26	T	N45	9.89	> −2.60	< 3.60	D
E16	0.888	> −3.74	< 3.69	T	G46	8.41	> −3.74	< 4.67	T
V17	0.308	> −3.74	< 3.23	T	R47	3.85	> −3.74	< 4.33	T
E18	0.488	> −2.62	< 2.31	H	I48	0.669	> −3.74	< 3.57	T
T19	1.31	> −2.60	< 2.72	D	L49	0.336	−3.94	3.46	T
K20	3.13	> −2.60	< 3.10	D	E50	0.416	> −2.60	< 2.22	D
S21	6.68	−2.85	3.68	H	N51	4.76	> −2.60	< 3.28	D
A22	4.32	> −2.60	< 3.24	D	G52	8.41	> −3.74	< 4.67	T
G23	4.03	> −2.60	< 3.21	D	E53	0.996	> −3.74	< 3.74	T
G24	5.96	> −2.60	< 3.38	D	V54	0.308	> −3.74	< 3.23	T
I25	0.596	−2.85	2.62	H	K55	1.43	−4.23	4.39	T
V26	0.255	> −2.60	< 2.01	D	P56	—	—	—	—
L27	0.413	> −2.60	< 2.22	D	L57	0.328	> −3.74	< 3.26	T
T28	1.14	> −2.60	< 2.66	D	D58	0.675	> −3.74	< 3.57	T
G29	6.38	> −2.60	< 3.41	D	V59	0.288	−4.75	4.21	T, D
S30	7.50	> −2.60	< 3.48	D	K60	1.43	−6.32	6.47	T
A31	4.32	> −2.60	< 3.24	D	V61	0.570	> −3.74	< 3.50	T

Residue	k_{int} (s^{-1})	log(k_{ex}/s^{-1})	log P_f	Methods[a]	Residue	k_{int} (s^{-1})	log(k_{ex}/s^{-1})	log P_f	Methods[a]
G62	2.92	−4.63	5.09	T, D	S75	6.68	> −3.74	< 4.57	T
D63	1.62	< −6.77	> 6.98	T	I78	0.532	> −3.74	< 3.47	T
I64	0.269	−6.52	5.95	T	D79	0.645	> −2.60	< 2.41	D
V65	0.255	−6.70	6.10	D	V83	0.308	−4.69	4.18	T
I66	0.293	n.a.	n.a		L84	0.413	−5.97	5.59	T, D
F67	0.734	−4.14	4.01	T	I85	0.249	−5.25	4.65	T
N68	7.67	> −3.74	< 4.63	T	M86	1.25	> −3.74	< 3.84	T
D69	2.29	> −2.60	< 2.96	D	S87	6.53	> −3.74	< 4.56	T
G70	2.68	> −2.60	< 3.03	D	E88	1.34	−3.11	3.24	D
Y71	1.72	> −2.60	< 3.83	D	S89	3.61	> −2.60	< 3.16	D
G72	4.52	> −2.60	< 3.25	D	D90	2.18	−4.49	4.83	D
V73	0.639	> −2.60	< 2.40	D	I91	0.269	−6.76	6.19	D
K74	1.43	> −3.74	< 3.90	T					

[a]The methods used to follow the H/D-exchange reactions were as follows: T, TROSY; D, DMSO-QHX; H, direct HSQC measurement. For the log(k_{ex}/s^{-1}) values measured by the two methods (T and D), the average values are shown.

[b]The H/D-exchange rate was too fast to measure, and the lower limit of log(k_{ex}/s^{-1}) and the upper limit of log P_f are shown.

[c]The H/D-exchange rate was too slow to measure, and the upper limit of log(k_{ex}/s^{-1}) and the lower limit of log P_f are shown.

Table 2. H/D-exchange parameters of GroES measured by TROSY at pH* 7.5 and 25°C[a]

Residue	k_{int} (s^{-1})	$\log(k_{ex}/s^{-1})$	log P_f
L6	3.27	−6.20	6.72
I11	2.92	−5.94	6.41
V12	2.54	−6.03	6.44
K13	14.3	−5.70	6.85
V40	3.06	−5.91	6.39
L41	4.12	−6.47	7.09
K60	14.3	−5.75	6.91
D63	16.0	−5.86	7.06
I64	2.66	−5.58	6.00
V65	2.54	−6.14	6.54
I66	2.92	−6.20	6.67
L84	4.12	−5.07	5.68
I91	2.66	−6.07	6.50

[a]The parameter values for slowly exchanging protons measured by TROSY are shown.

Chapter 4. Summary and future perspective

In conventional DMSO-QHX method, lyophilization was used to remove D_2O from the protein solution, and the lyophilized protein was dissolved in the DMSO solution (95% DMSO-d_6/5% D_2O, pH* 5.0) followed by analysis using NMR spectroscopy. However, this method has not been used for studies on fully unfolded proteins in a concentrated denaturant (6 M GdmCl or 8 M urea) or protein solutions at high salt concentrations because the denaturants or salts remain after lyophilization. In my studies, I replaced lyophilization step by the use of Zeba^{TM} spin desalting columns, and I successfully used this method to study ^{15}N labeled ubiquitin. I could analyze H/D-exchange kinetics for 12 amide protons and most of them were within the predicted exchange half time. Further, as 100% DMSO is often used to dissolve insoluble aggregates such as amyloid fibrils, I also used 100% DMSO to solubilize ^{15}N labeled ubiquitin powder, and the solvent (100% DMSO) was exchanged for the DMSO solution (95% DMSO-d_6/5% D_2O) for the measurement of the HSQC spectrum, and the spectrum thus obtained was identical to the spectrum previously obtained, indicating that this method is also applicable for water insoluble protein aggregates. Overall, the spin-column technique is less time consuming, and it can be applied for water soluble as well as water insoluble protein.

In Chapter 3, I used the above spin-column method to study a large protein assembly, i.e., free heptameric GroES. The large molecular weight (M_w= 73,000) of GroES makes it very difficult to investigate the H/D-exchange kinetics of the individual amide protons by the H/D-exchange techniques combined with conventional NMR spectroscopy. I thus successfully used an alternative approach to study the H/D-exchange kinetics of GroES, i.e., by TROSY and by DMSO-QHX followed by 2D NMR. As a result, I quantitatively evaluated the k_{ex} values of H/D-exchange for 33 out of the 94 peptide amide protons of GroES and their P_f values, and for the

remaining 61 residues, I obtained the lower and the upper limits of the k_{ex} and P_f values, respectively. I found that the flexible regions with weakly-protected amide protons ($P_f < 10^4$) were mostly located in the mobile loop region of GroES (residues 17–34), a reverse turn 49–52 at the top of the roof hairpin, and the region (strand E and the adjacent turns) between strands D and F. The highly protected residues with P_f values of 10^6–10^7 are located in the hydrophobic core region formed by strands B, C and D. A remarkable advantage of H/D-exchange studies is that we can directly evaluate the effective thermodynamic stability of a protein, without any theoretical models and extrapolations. I thus compared the P_f values for the most stable amide groups found in the core region of GroES, obtained by the H/D-exchange experiment, and the known results of the equilibrium unfolding transitions of GroES reported in the previous studies. The observed P_f values in the present studies are comparable in magnitude to those observed in typical small globular proteins, but the number of the highly protected amide protons with a P_f larger than 10^6 are significantly smaller than those reported for the small globular proteins, indicating that significant portions of GroES is flexible and natively unfolded. The average P_f value of the most highly protected residues, which form the hydrophobic core of GroES, was 6.7×10^6, which was much larger than the value expected from the two-state and three-state unfolding mechanisms previously reported, strongly suggesting that there are multiple intermediates during the equilibrium unfolding of GroES.

A further interesting issue concerning the structure and function of GroES may relate to the structural fluctuations of the GroES portion of the GroEL/GroES chaperonin complex. In the presence of ADP, the GroEL/GroES complex is formed,[12] and the complex is also formed in the presence of the ATP or in the presence of ADP-AlF_x.[15, 132] The GroEL/GroES/ATP and GroEL/GroES/ADP-AlF_x complexes are active, i.e., they can assist a stringent protein to fold into the native state, whereas the GroEL/GroES/ADP complex is unable to fold the protein into the native state. Surprisingly, the X- ray crystallographic structures of both the complexes are

essentially identical (PDB codes: 1AON, 1SVT and 1PCQ). Therefore, the studies on the structural fluctuations of these chaperonin complexes by the H/D-exchange techniques combined with NMR spectroscopy will give us clear insight into the apparently different biological activities of these chaperonin complexes. It has been reported that the single ring GroEL mutant, SR1, is sufficient to fold non-native proteins into the native state.[133] I thus performed a preliminary study on the H/D-exchange kinetics of the SR1/GroES/ADP complex. Although the H/D-exchange kinetics of the mobile loop residues (Thr19 and Gly24) of free GroES were too fast to measure with a k_{ex} value larger than 0.0025 s^{-1} at pH 6.5, the Thr19 and Gly24 residues gave k_{ex} values of 2.2×10^{-6} and 2.3×10^{-6} s^{-1}, respectively, in the SR1/GroES/ADP complex (Figure 4-1 (a) and (b)), indicating that the residues are highly protected in the complex with the P_f values of 6.0×10^{5} and 2.5×10^{6} for Thr19 and Gly24, respectively. Three residues, Ile11, Val59 and Asp90, the k_{ex} values of which were 2.2×10^{-7}, 1.9×10^{-5} and 3.2×10^{-5} s^{-1}, respectively, in free GroES, showed smaller k_{ex} values except for Ile 11, i.e., 2.5×10^{-6}, 1.3×10^{-6} s^{-1} and 5.8×10^{-6} s^{-1} for Ile11, Val59 and Asp90, suggesting that the residues in the core region of GroES were similarly or more protected in the SR1/GroES/ADP complex. The reason why Ile11 was 10-fold less protected in the complex than in free GroES remains unclear, but it is suggested that the subunit-subunit interface of GroES may become more flexible in the complex. The large change in the H/D-exchange protection found in the mobile loop of GroES also suggests that these residues play an important role in recognition of GroES by GroEL and structural stabilization of the GroEL/GroES complex. Further studies are required in future for elucidating relationships between structural fluctuations and differences in the biological functions of different GroEL/GroES/nucleotide complexes.

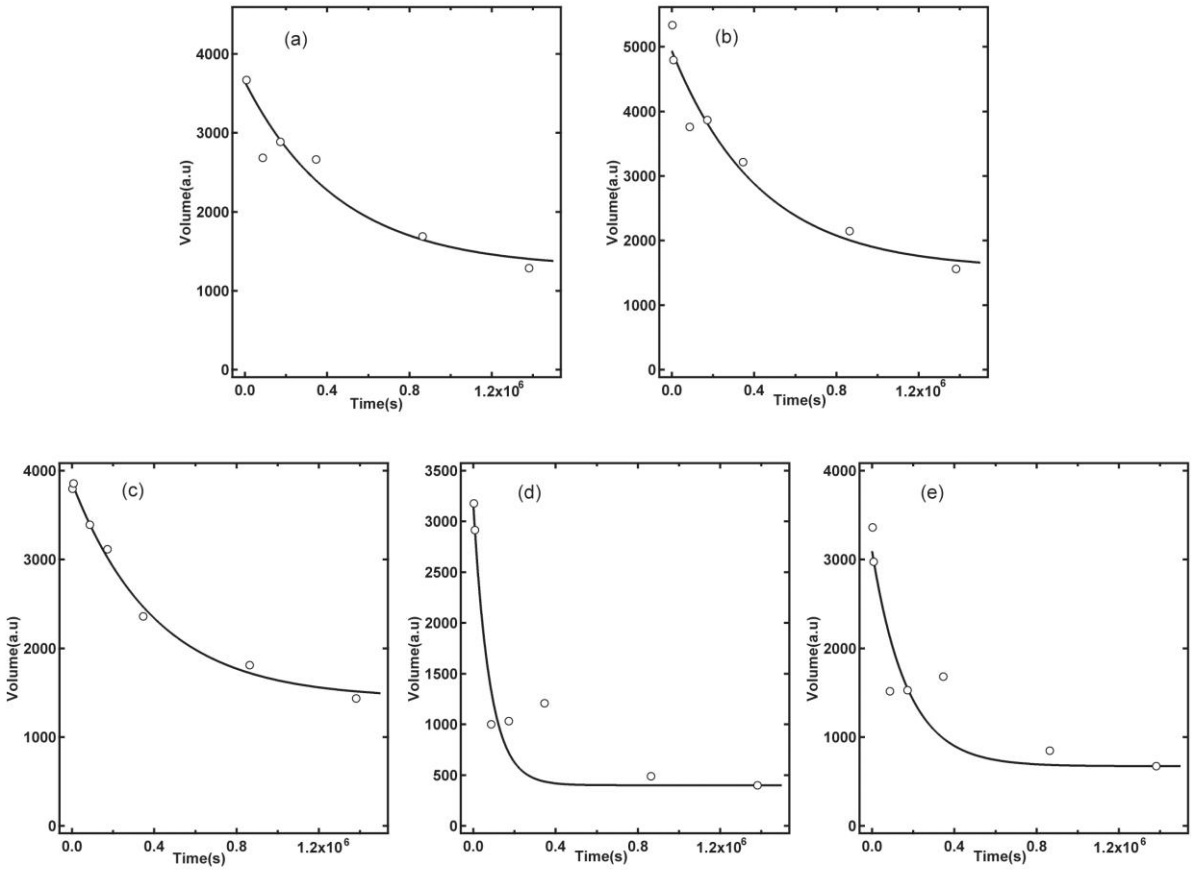

Figure 4-1. Kinetic progress curves of the H/D-exchange reactions of the GroES portion of the SR1/GroES complex monitored by DMSO-QHX ((a) and b)) indicate the H/D-exchange curves of the Thr19 and Gly24 amide protons of GroES (pH* 6.5 and 25°). ((c), (d) and (e)) indicate the H/D-exchange curves of the Ile11, Val59 and Asp90. The thick continuous lines are the theoretical exchange curves fitted to a single-exponential function (Equation (2-11). For the H/D-exchange experiments, a frozen stock GroES solution kept at −20°C was thawed, and the buffer was exchanged for Buffer C (50 mM bis-Tris, 10mM KCl and 25 mM $MgCl_2$ at pH 6.5) by the use of a dialysis bag. After adjusting the final GroES, SR1 and ADP concentration to 376 μM, 462 μM and 3 mM, respectively, ADP was added to SR1 followed by the addition of GroES, and the mixture was passed through a PD10 desalting column equilibrated with the solution that contained the components of Buffer C and 3 mM ADP prepared in D_2O (pH* 6.5), giving the final GroES and SR1 concentration of 200 and 300 μM, respectively, in monomer units. The rest of the methods were the same as described in Chapter 3,[57] and I collected the samples with pre-determined exchange times between 30 min and 10 days. For the NMR measurement, the frozen sample was first thawed at room temperature, and the medium containing Buffer B in 90%D_2O/10%H_2O was exchanged for the DMSO solution

(95% DMSO-d_6/5% D_2O and pH* 5.0) by using a spin desalting column (Zeba^{TM} Spin Desalting Column 89891, 5 mL; Thermo Scientific) as described Chapter 2. The $^{1}H–^{15}N$ HSQC spectrum of the protein in the DMSO solution was measured on a Bruker Avance 500 NMR spectrometer at 25 °C.

Acknowledgements

My PhD studies completion has been due to the continuous guidance, encouragement and support of several people to whom I would like to express my gratitude.

I am especially thankful to my thesis advisor Professor Kunihiro Kuwajima for his suggestions, valuable guidance, encouragement, discussions and for thorough reading of this dissertation work. He has also helped me to develop my research background in the field of Protein Science. I am extremely grateful to Professor Koichi Kato for his help, timely guidance and reading of this dissertation.

My heartfelt gratitude to Dr. Takashi Nakamura, Dr. Koki Makabe who helped me in conducting my research, taught me necessary skills and shared their abundant scientific knowledge which was vital for me to deal with experiential training. I am thankful to Dr. Toshio Takenka for his expertise and time to train me in conducting experiments. Dr. Atsushi Mukaiyama and Dr. Jin Chen who guided me through rewarding discussions are greatly acknowledged. Ms. Michiko Nakano who carried out NMR measurement, Ms. Kei Tanaka and Mrs. Hiroko Mizuki, who helped me in official documentations are highly appreciated. I also thank to Dr. Takumi Yamaguchi and Dr. Maho Yagi-Utsumi, who helped me in thesis documentation and shared their scientific knowledge with discussions.

I am highly obliged to The Ministry of Education, Culture, Sports, Science, and Technology of Japan for offering me financial support during my PhD studies. I sincerely appreciate the efforts of the examiners of this thesis Prof. Shigetoshi Aono, Prof. Shuji Akiyama, Prof. Yuji Goto, Prof. Yuji Furutani for their critical readings, analysis of thesis and valuable suggestions.

Finally, I would like to offer my special thanks to my parents Mr. Shantilalji Chandak and Mrs. Mangal Chandak, and my brothers Mr. Satish Chandak and Mr. Dinesh Chandak for their affection, encouragement, understanding, patience and faith, which helped me to successfully complete a big milestone in my professional life.

Thank you!

References

[1]. Epstein CJ, Goldberger RF, Anfinsen CB. Genetic control of tertiary protein structure – Studies with model system. *Cold Spring Harbor Symposia On Quantitative Biology* 1963; **28**:439.

[2]. Levinthal C. Are there pathways for protein folding? *Journal de Chimie Physique et de Physico-Chimie Biologique* 1968;**65**:44-5.

[3]. Udgaonkar JB. Polypeptide chain collapse and protein folding. *Arch Biochem Biophys* 2013;**531**(1-2):24-33.

[4]. Bryngelson JD, Onuchic JN, Socci ND, Wolynes PG. Funnels, pathways, and the energy landscape of protein folding: a synthesis. *Proteins* 1995;**21**(3):167-95.

[5]. Zimmerman SB, Minton AP. Macromolecular crowding: biochemical, biophysical, and physiological consequences. *Annu Rev Biophys Biomol Struct* 1993;**22**:27-65.

[6]. Martin J, Hartl FU. Protein folding in the cell: molecular chaperones pave the way. *Structure (Camb)* 1993;**1**(3):161-4.

[7]. Hartl FU. Molecular chaperones in cellular protein folding. *Nature* 1996;**381**:571-80.

[8]. Kim Y, Hipp M, Bracher A, Hayer-Hartl M, Ulrich Hartl F. Molecular chaperone functions in protein folding and proteostasis. *Annu Rev Biochem* 2013;**82**:323-55.

[9]. Spiess C, Meyer A, Reissmann S, Frydman J. Mechanism of the eukaryotic chaperonin: protein folding in the chamber of secrets. *Trends Cell Biol* 2004;**14**(11):598-604.

[10]. Meyer AS, Gillespie JR, Walther D, Millet IS, Doniach S, Frydman J. Closing the folding chamber of the eukaryotic chaperonin requires the transition state of ATP hydrolysis. *Cell* 2003;**113**(3):369-81.

[11]. Ditzel L, Loewe J, Stock D *et al*. Crystal structure of the thermosome, the archaeal chaperonin and homolog of CCT. *Cell* 1998;**93**:125-38.

[12]. Xu ZH, Horwich AL, Sigler PB. The crystal structure of the asymmetric GroEL-GroES-$(ADP)_7$ chaperonin complex. *Nature* 1997;**388**:741-50.

[13]. Kerner MJ, Naylor DJ, Ishihama Y *et al*. Proteome-wide analysis of chaperonin-dependent protein folding in *Escherichia coli*. *Cell* 2005;**122**(2):209-20.

[14]. Burston SG, Ranson NA, Clarke AR. The origins and consequences of asymmetry in the chaperonin reaction cycle. *J Mol Biol* 1995;**249**:138-52.

[15]. Inobe T, Kikushima K, Makio T, Arai M, Kuwajima K. The allosteric transition of GroEL induced by metal fluoride-ADP complexes. *J Mol Biol* 2003;**329**(1):121-34.

[16]. Ewalt KL, Hendrick JP, Houry WA, Hartl FU. *In vivo* observation of polypeptide flux through the bacterial chaperonin system. *Cell* 1997;**90**:491-500.

[17]. Sigler PB, Xu ZH, Rye HS, Burston SG, Fenton WA, Horwich AL. Structure and function in GroEL-mediated protein folding. *Annu Rev Biochem* 1998;**67**:581-608.

[18]. Braig K, Otwinowski Z, Hegde R *et al*. The crystal structure of the bacterial chaperonin GroEL at 2.8 Å. *Nature* 1994;**371**:578-86.

[19]. Hunt JF, Weaver AJ, Landry SJ, Gierasch L, Deisenhofer J. The crystal structure of the GroES co-chaperonin at 2.8 Å resolution. *Nature* 1996;**379**:37-45.

[20]. Fiaux J, Bertelsen EB, Horwich AL, Wüthrich K. NMR analysis of a 900K GroEL GroES complex. *Nature* 2002;**418**(6894):207-11.

[21]. Horst R, Wider G, Fiaux J, Bertelsen E, Horwich A, Wüthrich K. Proton-proton overhauser NMR spectroscopy with polypeptide chains in large structures. *Proc Natl Acad Sci U S A* 2006;**103**(42):15445-50.

[22]. Chen D, Madan D, Weaver J *et al*. Visualizing GroEL/ES in the act of encapsulating a folding protein. *Cell* 2013;**153**(6):1354-65.

[23]. Martin J, Mayhew M, Langer T, Hartl FU. The reaction cycle of GroEL and GroES in chaperonin-assisted protein folding. *Nature* 1993;**366**:228-33.

[24]. Langer T, Pfeifer G, Martin J, Baumeister W, Hartl FU. Chaperonin-mediated protein folding: GroES binds to one end of the GroEL cylinder, which accommodates the protein substrate within its central cavity. *EMBO J* 1992;**11**:4757-65.

[25]. Sameshima T, Ueno T, Lizuka R *et al*. Football- and bullet-shaped GroEL-GroES complexes coexist during the reaction cycle. *J Biol Chem* 2008;**283**(35):23765-73.

[26]. Todd MJ, Viitanen PV, Lorimer GH. Dynamics of the chaperonin ATPase cycle: Implications for facilitated protein folding. *Science* 1994;**265**:659-66.

[27]. Hartl FU, Hayer-Hartl M. Converging concepts of protein folding *in vitro* and *in vivo*. *Nat Struct Mol Biol* 2009;**16**(6):574-81.

[28]. Clare D, Vasishtan D, Stagg S *et al*. ATP-triggered conformational changes delineate substrate-binding and -folding mechanics of the GroEL chaperonin. *Cell* 2012;**149**(1):113-23.

[29]. Weissman J, Hohl C, Kovalenko O *et al*. Mechanism of GroEL action: productive release of polypeptide from a sequestered position under GroES. *Cell* 1995;**83**(4):577-87.

[30]. Viitanen PV, Gatenby AA, Lorimer GH. Purified chaperonin 60 (GroEL) interacts with the nonnative states of a multitude of *Escherichia coli* proteins. *Protein Sci* 1992;**1**(3):363-9.

[31]. Braig K, Adams PD, Bruenger AT. Conformational variability in the refined structure of the chaperonin GroEL at 2.8 Å resolution. *Nature Struct Biol* 1995;**2**:1083-94.

[32]. Li Y, Gao X, Chen L. GroEL recognizes an amphipathic helix and binds to the hydrophobic side. *J Biol Chem* 2009;**284**(7):4324-31.

[33]. Fenton WA, Kashi Y, Furtak K, Horwich AL. Residues in chaperonin GroEL required for polypeptide binding and release. *Nature* 1994;**371**:614-9.

[34]. Weissman JS, Kashi Y, Fenton WA, Horwich AL. GroEL-mediated protein folding proceeds by multiple rounds of binding and release of nonnative forms. *Cell* 1994;**78**:693-702.

[35]. Yifrach O, Horovitz A. Nested cooperativity in the ATPase activity of the oligomeric chaperonin GroEL. *Biochemistry* 1995;**34**(16):5303-8.

[36]. Horowitz PM, Lorimer GH, Ybarra J. GroES in the asymmetric $GroEL_{14}$-$GroES_7$ complex exchanges via an associative mechanism. *Proc Natl Acad Sci U S A* 1999;**96**(6):2682-6.

[37]. Fenton W, Horwich AL. GroEL-mediated protein folding. Review. *Protein Sci* 1997;**6**(4):743-60.

[38]. Ellis RJ. Protein folding: importance of the anfinsen cage. Review. *Curr Biol* 2003;**13**(22):R881-3.

[39]. Sameshima T, Iizuka R, Ueno T *et al*. Single-molecule study on the decay process of the football-shaped GroEL-GroES complex using zero-mode waveguides. *J Biol Chem* 2010;**285**(30):23159-64.

[40]. Hoshino M, Katou H, Yamaguchi KI, Goto Y. Dimethylsulfoxide-quenched hydrogen/deuterium exchange method to study amyloid fibril structure. *Biochim Biophys Acta* 2007;**1768**(8):1886-99.

[41]. Clarke J, Itzhaki LS. Hydrogen exchange and protein folding. *Curr Opin Struct Biol* 1998;**8**:112-8.

[42]. Englander S, Downer N, Teitelbaum H. Hydrogen exchange. Review. *Annu Rev Biochem* 1972;**41**:903-24.

[43]. Bai Y, Milne JS, Mayne L, Englander SW. Primary structure effects on peptide group hydrogen exchange. *Proteins* 1993;**17**:75-86.

[44]. Connelly GP, Bai Y, Jeng MF, Englander SW. Isotope effects in peptide group hydrogen exchange. *Proteins* 1993;**17**:87-92.

[45]. Englander S, Kallenbach N. Hydrogen exchange and structural dynamics of proteins and nucleic acids. *Q Rev Biophys* 1983;**16**(4):521-655.

[46]. Bai Y, Sosnick TR, Mayne L, Englander SW. Protein folding intermediates: native-state hydrogen exchange. *Science* 1995;**269**:192-7.

[47]. Bai Y. Protein folding pathways studied by pulsed and native-state hydrogen exchange. *Chem Rev* 2006;**106**(5):1757-68.

[48]. Maity H, Lim WK, Rumbley JN, Englander SW. Protein hydrogen exchange mechanism: local fluctuations. *Protein Sci* 2003;**12**(1):153-60.

[49]. Wani A, Udgaonkar JB. Native state dynamics drive the unfolding of the SH3 domain of PI3 kinase at high denaturant concentration. *Proc Natl Acad Sci U S A* 2009;**106**(49):20711-6.

[50]. Arai M, Kuwajima K. Rapid formation of a molten globule intermediate in refolding of α-lactalbumin. *Fold Des* 1996;**1**(4):275-87.

[51]. Hughson FM, Wright PE, Baldwin RL. Structural characterization of a partly folded apomyoglobin intermediate. *Science* 1990;**249**:1544-8.

[52]. Bai Y, Milne JS, Mayne L, Englander SW. Protein stability parameters measured by hydrogen exchange. *Proteins* 1994;**20**:4-14.

[53]. Bodenhausen G, Ruben DJ. Natural abundance nitrogen-15 NMR by enhanced heteronuclear spectroscopy. *Chem Phys Lett* 1980;**69**(1):185-9.

[54]. Berger S, Facke T, Wagner R. Two-dimensional correlation spectroscopy by scalar couplings: A walk through the periodic table. *Magn Reson Chem* 1996;**34**:4-13.

[55]. Riek R, Pervushin K, Wüthrich K. TROSY and CRINEPT: NMR with large molecular and supramolecular structures in solution. *Curr Opin Struct Biol* 2000;**25**(10):462-8.

[56]. Fernandez C, Wider G. TROSY in NMR studies of the structure and function of large biological macromolecules. *Curr Opin Struct Biol* 2003;**13**(5):570-80.

[57]. Chandak MS, Nakamura T, Takenaka T *et al*. The use of spin desalting columns in DMSO-quenched H/D-exchange NMR experiments. *Protein Sci* 2013; 22(4):486-91

[58]. Zhang YZ, Paterson Y, Roder H. Rapid amide proton exchange rates in peptides and proteins measured by solvent quenching and two-dimensional NMR. *Protein Sci* 1995;**4**:804-14.

[59]. Alexandrescu AT. An NMR-based quenched hydrogen exchange investigation of model amyloid fibrils formed by cold shock protein A. *Pac Symp Biocomput* 2001;:67-78.

[60]. Hoshino M, Katou H, Hagihara Y, Hasegawa K, Naiki H, Goto Y. Mapping the core of the β_2-microglobulin amyloid fibril by H/D exchange. *Nature Structural Biology* 2002;**9**(5):332-6.

[61]. Ippel JH, Olofsson A, Schleucher J, Lundgren E, Wijmenga SS. Probing solvent accessibility of amyloid fibrils by solution NMR spectroscopy. *Proc Natl Acad Sci U S A* 2002;**99**(13):8648-53.

[62]. Kuwata K, Matumoto T, Cheng H, Nagayama K, James TL, Roder H. NMR-detected hydrogen exchange and molecular dynamics simulations provide structural insight into fibril formation of prion protein fragment 106-126. *Proc Natl Acad Sci U S A* 2003;**100**(25):14790-5.

[63]. Yamaguchi KI, Katou H, Hoshino M, Hasegawa K, Naiki H, Goto Y. Core and heterogeneity of β_2-microglobulin amyloid fibrils as revealed by H/D exchange. *J Mol Biol* 2004;**338**(3):559-71.

[64]. Carulla N, Caddy GL, Hall DR *et al*. Molecular recycling within amyloid fibrils. *Nature* 2005;**436**(7050):554-8.

[65]. Whittemore NA, Mishra R, Kheterpal I, Williams AD, Wetzel R, Serpersu EH. Hydrogen-deuterium (H/D) exchange mapping of Aβ $_{1-40}$ amyloid fibril secondary structure using nuclear magnetic resonance spectroscopy. *Biochemistry* 2005;**44**(11):4434-41.

[66]. Dyson HJ, Kostic M, Liu J, Martinez-Yamout MA. Hydrogen-deuterium exchange strategy for delineation of contact sites in protein complexes. *FEBS Lett* 2008;**582**(10):1495-500.

[67]. Chakraborty S, Hosur RV. NMR insights into the core of GED assembly by H/D-exchange coupled with DMSO dissociation and analysis of the denatured state. *J Mol Biol* 2011;**405**(5):1202-14.

[68]. Nishimura C, Dyson HJ, Wright PE. Enhanced picture of protein-folding intermediates using organic solvents in H/D-exchange and quench-flow experiments. *Proc Natl Acad Sci U S A* 2005;**102**(13):4765-70.

[69]. Nishimura C, Dyson HJ, Wright PE. The kinetic and equilibrium molten globule intermediates of apoleghemoglobin differ in structure. *J Mol Biol* 2008;**378**(3):715-25.

[70]. Sakamoto K, Hirai K, Kitamura Y *et al*. Glycerol-induced folding of unstructured disulfide-deficient lysozyme into a native-like conformation. *Biopolymers* 2009;**91**(8):665-75.

[71]. Loftus D, Gbenle GO, Kim PS, Baldwin RL. Effects of denaturants on amide proton-exchange rates - a test for structure in protein-fragments and folding intermediates. *Biochemistry* 1986;**25**(6):1428-36.

[72]. Ibarra-Molero B, Loladze VV, Makhatadze GI, Sanchez R. Thermal versus guanidine-induced unfolding of ubiquitin- an analysis in terms of the contributions from charge-charge interactions to protein stability. *Biochemistry* 1999;**38**(25):8138-49.

[73]. Yagi-Utsumi M, Matsuo K, Yanagisawa K, Gekko K, Kato K. Spectroscopic Characterization of intermolecular interaction of amyloid β Promoted on GM1 Micelles. *Int J Alzheimers Dis* 2011;:925073.

[74]. Zhang H, Neal S, Wishart DS. RefDB: a database of uniformly referenced protein chemical shifts. *J Biomol NMR* 2003;**25**(3):173-95.

[75]. Delaglio F, Grzesiek S, Vuister GW, Zhu G, Pfeifer J, Bax A. NMRPipe: a multidimensional spectral processing system based on UNIX pipes. *J Biomol NMR* 1995;**6**(3):277-93.

[76]. Johnson BA, Blevins RA. NMR View: A computer program for the visualization and analysis of NMR data. *J Biomol NMR* 1994;**4**(5):603-14.

[77]. Fenton WA, Weissman JS, Horwich AL. Putting a lid on protein folding: structure and function of the co-chaperonin, GroES. *Chem Biol* 1996;**3**(3):157-61.

[78]. Chaudhuri TK, Verrna VK, Maheshwari A. GroEL assisted folding of large polypeptide substrates in *Escherichia coli*: present scenario and assignments for the future. *Prog Biophys Mol Biol* 2009;**99**(1):42-50.

[79]. Horwich AL, Fenton WA. Chaperonin-mediated protein folding: using a central cavity to kinetically assist polypeptide chain folding. *Q Rev Biophys* 2009;**42**(2):83-116.

[80]. Thirumalai D, Lorimer GH. Chaperonin-mediated protein folding. *Annu Rev Biophys Biomol Struct* 2001;**30**:245-69.

[81]. Tang YC, Chang HC, Roeben A *et al*. Structural features of the GroEL-GroES nano-cage required for rapid folding of encapsulated protein. *Cell* 2006;**125**(5):903-14.

[82]. Katsumata K, Okazaki A, Kuwajima K. Effect of GroEL on the re-folding kinetics of α-lactalbumin. *J Mol Biol* 1996;**258**(5):827-38.

[83]. Okazaki A, Katsumata K, Kuwajima K. Hydrogen-exchange kinetics of reduced α-lactalbumin bound to the chaperonin GroEL. *J Biochem (Tokyo)* 1997;**121**:534-41.

[84]. Makio T, Arai M, Kuwajima K. Chaperonin-affected refolding of α-lactalbumin: effects of nucleotides and the co-chaperonin GroES. *J Mol Biol* 1999;**293**(1):125-37.

[85]. Cliff MJ, Kad NM, Hay N *et al*. A kinetic analysis of the nucleotide-induced allosteric transitions of GroEL. *J Mol Biol* 1999;**293**(3):667-84.

[86]. Inobe T, Makio T, Takasu-Ishikawa E, Terada TP, Kuwajima K. Nucleotide binding to the chaperonin GroEL: non-cooperative binding of ATP analogs and ADP, and cooperative effect of ATP. *Biochim Biophys Acta* 2001;**1545**:160-73.

[87]. Inobe T, Arai M, Nakao M *et al*. Equilibrium and kinetics of the allosteric transition of GroEL studied by solution X-ray scattering and fluorescence spectroscopy. *J Mol Biol* 2003;**327**(1):183-91.

[88]. Inobe T, Kuwajima K. Φ-value analysis of an allosteric transition of GroEL based on a single-pathway model. *J Mol Biol* 2004;**339**(1):199-205.

[89]. Horovitz A, Willison KR. Allosteric regulation of chaperonins. *Curr Opin Struct Biol* 2005;**15**(6):646-51.

[90]. Grason JP, Gresham JS, Lorimer GH. Setting the chaperonin timer: a two-stroke, two-speed, protein machine. *Proc Natl Acad Sci U S A* 2008;**105**(45):17339-44.

[91]. Inobe T, Takahashi K, Maki K *et al*. Asymmetry of the GroEL-GroES complex under physiological conditions as revealed by small-angle x-ray scattering. *Biophys J* 2008;**94**(4):1392-402.

[92]. Chakraborty K, Chatila M, Sinha J *et al*. Chaperonin-catalyzed rescue of kinetically trapped states in protein folding. *Cell* 2010;**142**(1):112-22.

[93]. Motojima F, Yoshida M. Polypeptide in the chaperonin cage partly protrudes out and then folds inside or escapes outside. *EMBO J* 2010;**29**(23):4008-19.

[94]. Kovacs E, Sun Z, Liu H *et al*. Characterisation of a GroEL single-ring mutant that supports growth of *Escherichia coli* and has GroES-dependent ATPase activity. *J Mol Biol* 2010;**396**(5):1271-83.

[95]. Chen J, Makabe K, Nakamura T, Inobe T, Kuwajima K. Dissecting a bimolecular process of $MgATP_2$-binding to the chaperonin GroEL. *J Mol Biol* 2011;**410**(2):343-56.

[96]. Motojima F, Motojima-Miyazaki Y, Yoshida M. Revisiting the contribution of negative charges on the chaperonin cage wall to the acceleration of protein folding. *Proc Natl Acad Sci U S A* 2012;**109**(39):15740-5.

[97]. Landry SJ, Zeilstra-Ryalls J, Fayet O, Georgopoulos C, Gierasch LM. Characterization of a functionally important mobile domain of GroES. *Nature* 1993;**364**(6434):255-8.

[98]. Landry SJ, Taher A, Georgopoulos C, Van der Vies SM. Interplay of structure and disorder in cochaperonin mobile loops. *Proc Natl Acad Sci U S A* 1996;**93**:11622-7.

[99]. Shewmaker F, Maskos K, Simmerling C, Landry SJ. The disordered mobile loop of GroES folds into a defined β-hairpin upon binding GroEL. *J Biol Chem* 2001;**276**(33):31257-64.

[100]. Shewmaker F, Kerner MJ, Hayer-Hartl M, Klein G, Georgopoulos C, Landry SJ. A mobile loop order-disorder transition modulates the speed of chaperonin cycling. *Protein Sci* 2004;**13**(8):2139-48.

[101]. Chaudhry C, Horwich AL, Brunger AT, Adams PD. Exploring the structural dynamics of the *E. coli* chaperonin GroEL using translation-libration-screw crystallographic refinement of intermediate states. *J Mol Biol* 2004;**342**(1):229-45.

[102]. Nishida N, Motojima F, Idota M *et al*. Probing dynamics and conformational change of the GroEL-GroES complex by ^{13}C NMR spectroscopy. *J Biochem (Tokyo)* 2006;**140**(4):591-8.

[103]. Hyeon C, Lorimer GH, Thirumalai D. Dynamics of allosteric transitions in GroEL. *Proc Natl Acad Sci U S A* 2006;**103**(50):18939-44.

[104]. Illingworth M, Ramsey A, Zheng Z, Chen L. Stimulating the substrate folding activity of a single ring GroEL variant by modulating the cochaperonin GroES. *J Biol Chem* 2011;**286**(35):30401-8.

[105]. Zhang Q, Chen J, Kuwajima K *et al*. Nucleotide-induced conformational changes of tetradecameric GroEL mapped by hydrogen/deuterium exchange monitored by FT-ICR mass spectrometry. *Scientific Reports* 2013; 3:1247.

[106]. Pervushin K, Riek R, Wider G, Wüthrich K. Attenuated T_2 relaxation by mutual cancellation of dipole-dipole coupling and chemical shift anisotropy indicates an avenue to NMR structures of very large biological macromolecules in solution. *Proc Natl Acad Sci U S A* 1997;**94**(23):12366-71.

[107]. Riek R, Fiaux J, Bertelsen EB, Horwich AL, Wüthrich K. Solution NMR techniques for large molecular and supramolecular structures. *J Am Chem Soc* 2002;**124**(41):12144-53.

[108]. Chaudhry C, Farr GW, Todd MJ *et al*. Role of the γ-phosphate of ATP in triggering protein folding by GroEL-GroES: function, structure and energetics. *EMBO J* 2003;**22**(19):4877-87.

[109]. Seale JW, Gorovits BM, Ybarra J, Horowitz PM. Reversible oligomerization and denaturation of the chaperonin GroES. *Biochemistry* 1996;**35**:4079-83.

[110]. Boudker O, Todd MJ, Freire E. The structural stability of the co-chaperonin GroES. *J Mol Biol* 1997;**272**:770-9.

[111]. Higurashi T, Nosaka K, Mizobata T, Nagai J, Kawata Y. Unfolding and refolding of *Escherichia coli* chaperonin GroES is expressed by a three-state model. *J Mol Biol* 1999;**291**(3):703-13.

[112]. Sakane I, Ikeda M, Matsumoto C *et al*. Structural stability of oligomeric chaperonin 10: the role of two β-strands at the N and C termini in structural stabilization. *J Mol Biol* 2004;**344**(4):1123-33.

[113]. Luke K, Wittung-Stafshede P. Folding and assembly pathways of co-chaperonin proteins 10: Origin of bacterial thermostability. *Arch Biochem Biophys* 2006;**456**(1):8-18.

[114]. Higurashi T, Hiragi Y, Ichimura K *et al*. Structural stability and solution structure of chaperonin GroES heptamer studied by synchrotron small-angle x-ray scattering. *J Mol Biol* 2003;**333**(3):605-20.

[115]. Herendeen SL, VanBogelen RA, Neidhardt FC. Levels of major proteins of *Escherichia coli* during growth at different temperatures. *J Bacteriol* 1979;**139**(1):185-94.

[116]. Lorimer GH. A quantitative assessment of the role of chaperonin proteins in protein folding *in vivo*. *FASEB J* 1996;**10**:5-9.

[117]. Ellis RJ, Hartl FU. Protein folding in the cell: competing models of chaperonin function. *FASEB J* 1996;**10**:20-6.

[118]. Kabsch W, Sander C. Dictionary of protein secondary structure: pattern recognition of hydrogen-bonded and geometrical features. *Biopolymers* 1983;**22**:2577-637.

[119]. Huyghues-Despointes BM, Pace CN, Englander SW, Scholtz JM. Measuring the conformational stability of a protein by hydrogen exchange. *Methods Mol Biol* 2001;**168**:69-92.

[120]. Skinner JJ, Lim WK, Bedard S, Black BE, Englander SW. Protein hydrogen exchange: testing current models. *Protein Sci* 2012;**21**(7):987-95.

[121]. Huyghues-Despointes BMP, Scholtz JM, Pace CN. Protein conformational stabilities can be determined from hydrogen exchange rates. *Nat Struct Biol* 1999;**6**(10):910-2.

[122]. Perrett S, Clarke J, Hounslow AM, Fersht AR. Relationship between equilibrium amide proton exchange behavior and the folding pathway of barnase. *Biochemistry* 1995;**34**:9288-98.

[123]. Englander SW, Mayne L, Krishna MMG. Protein folding and misfolding: mechanism and principles. *Q Rev Biophys* 2007;**40**(4):287-326.

[124]. Zondlo J, Fisher KE, Lin ZL, Ducote KR, Eisenstein E. Monomer-heptamer equilibrium of the *Escherichia coli* chaperonin GroES. *Biochemistry* 1995;**34**:10334-9.

[125]. Skinner JJ, Lim WK, Bedard S, Black BE, Englander SW. Protein dynamics viewed by hydrogen exchange. *Protein Sci* 2012;**21**(7):996-1005.

[126]. Seale JW, Horowitz PM. The C-terminal sequence of the chaperonin GroES is required for oligomerization. *J Biol Chem* 1995;**270**:30268-70.

[127]. Park C, Marqusee S. Analysis of the stability of multimeric proteins by effective ΔG and effective m-values. *Protein Sci* 2004;**13(**9):2553-8.

[128]. Creighton TE. Proteins: Structures and Molecular Properties, Second Edition. *W H Freeman and Company, New York* 1993.

[129]. Santoro MM, Bolen DW. A test of the linear extrapolation of unfolding free energy changes over an Extended denaturant concentration range. *Biochemistry* 1992;**31**:4901-7.

[130]. Sakane K, Hongo K, Mizobata T, Kawata Y. Mechanical unfolding of covalently linked GroES: Evidence of structural subunit intermediates. *Protein Sci* 2009;**18**(1):252-7.

[131]. Ikeda-Kobayashi A, Taniguchi Y, Brockwell DJ, Paci E, Kawakami M. Prying open single GroES ring complexes by force reveals cooperativity across domains. *Biophys J* 2012;**102**(8):1961-8.

[132]. Boisvert DC, Wang J, Otwinowski Z, Horwich AL, Sigler PB. The 2.4 Å crystal structure of the bacterial chaperonin GroEL complexed with ATPγS. *Nat Struct Biol* 1996;**3**(2):170-7.

[133]. Nielsen KL, Cowan NJ. A single ring is sufficient for productive chaperonin-mediated folding *in vivo*. *Mol Cell* 1998;**2**(1):93-9.